

1 **Age-related Macular Degeneration patient deep phenotyping and**
2 **whole genome sequencing analysis identifies coding variants linking**
3 **small low-luminance visual deficit to fat storage defects**
4

5
6 Sehyun Kim,^{1,7} Amy Stockwell,² Han Qin,¹ Simon S. Gao,³ Meredith Sagolla,⁴ Ivaylo
7 Stoilov,⁵ Arthur Wuster,^{2,8} Phillip Lai,⁶ Brian L. Yaspan,^{2,9} Marion Jeanne,^{1,9,*}
8

9 ¹ Department of Neuroscience, Genentech Inc., South San Francisco, CA 94080, USA

10 ² Department of Human Genetics, Genentech Inc., South San Francisco, CA 94080, USA

11 ³ Department of Clinical Imaging, Genentech Inc., South San Francisco, CA 94080, USA

12 ⁴ Department of Research Pathology, Genentech Inc., South San Francisco, CA 94080, USA

13 ⁵ Medical Affairs Ophthalmology, Genentech Inc., South San Francisco, CA 94080, USA

14 ⁶ Early Clinical Development, Genentech Inc., South San Francisco, CA 94080, USA
15

16 Present addresses:

17 ⁷ ABL Bio Inc., Seongnam, Republic of Korea

18 ⁸ Department of Translational Genomics, BioMarin Pharmaceutical, San Rafael, CA 94901,
19 USA
20

21 ⁹ The authors wish it to be known that, in their opinion, the last two authors should be
22 regarded as joint Senior Authors
23

24 * Corresponding author: email: jeanne.marion@gene.com
25

26 **Abstract**

27 **Background:** The basis of Age-related macular degeneration (AMD) genetic risk has been well
28 documented; however, few studies have looked at genetic biomarkers of disease progression or
29 treatment response within advanced AMD patients. Here we report the first genome-wide
30 analysis of genetic determinants of low-luminance vision deficit (LLD), which is seen as
31 predictive of visual acuity loss and anti-VEGF treatment response in neovascular AMD
32 patients.

33 **Methods:** AMD patients were separated into small- and large-LLD groups for comparison and
34 whole genome sequencing was performed. Genetic determinants of LLD were assessed by
35 common and rare variant genetic analysis. Follow-up functional analysis of rare coding variants
36 identified by the burden test was then performed *in vitro*.

37 **Results:** We identified four coding variants in the *CIDEA* gene. These rare variants were only
38 present in patients with a small LLD, which has been previously shown to indicate better
39 prognosis and better treatment response. Our *in vitro* functional characterization of these
40 *CIDEA* alleles revealed that all decrease the binding affinity between CIDEA and the lipid
41 droplet fusion effectors PLIN1, RAB8A and AS160. The rare *CIDEA* alleles all cause a
42 hypomorphic defect in lipid droplet fusion and enlargement, resulting in a decreased fat storage
43 capability in adipocytes.

44 **Conclusions:** As we did not detect CIDEA expression in the ocular tissue affected by AMD,
45 our results suggest that the *CIDEA* variants do not play a direct role in the eye and influence
46 low-luminance vision deficit via an indirect and systemic effect related to fat storage capacity.

47 **Funding:** No external funding was received for this work.

48

49

50 **Introduction**

51 Age-related macular degeneration (AMD) accounts for nearly 10% of blindness
52 worldwide, and is the leading cause of blindness in developed countries¹. AMD is a progressive
53 retinal disease characterized by the accumulation of extracellular deposits called drusen,
54 underneath the retina in the early stages of the disease, followed by either atrophy of the macula
55 in the advanced dry form of AMD called Geographic Atrophy (GA), and/or growth of
56 pathogenic blood vessels into the retina in the wet form of AMD called neovascular AMD. Both
57 GA and neovascular AMD are clinical end-stages forms of AMD and lead to progressive and
58 severe vision loss. There is currently no approved treatment for GA and despite anti-Vascular
59 Endothelial Growth Factor (VEGF) intraocular injections having revolutionized the treatment
60 of neovascular AMD, they are not curative and patient response is heterogeneous².

61 Although the pathophysiology of AMD is still not completely understood, there is a
62 well-established genetic component to disease risk. Concordance rates between mono-zygotic
63 twins are significantly higher than di-zygotic twins³⁻⁵. Both population-based and familial
64 studies have found evidence of sibling correlations, and estimate that genetic factors can
65 account for between 50% and 70% of the total variability in disease risk^{6;7}. Furthermore, it is
66 estimated that genetic risk factors account for up to 71% of variation in the severity of disease
67⁸. Genome-wide association studies (GWAS) of AMD disease risk have greatly expanded our
68 knowledge around the disease and especially its biology, with the most recent study involving
69 over 16,000 AMD patients and 17,000 controls finding 52 independently associated variants⁹.
70 Major risk loci identified include complement genes (e.g. *CFH*, *CFI*, *C3*, *C9*) and the
71 *ARMS2/HTRA1* locus. However, there are several other pathways identified including genes
72 involved in lipid metabolism (e.g. *LIPC*, *CETP*) and extracellular matrix remodeling (e.g.
73 *TIMP3*, *MMP9*).

74 While the basis of genetic risk of AMD is well characterized, other facets of the disease
75 are not. Predictive or prognostic biomarkers, either clinical or genetic, for disease progression
76 or treatment response are not as well understood. It is known that subjects with AMD have
77 difficulty seeing in dimly lit environments ¹⁰. As such, the reduction in visual acuity under
78 suboptimal illumination known as low-luminance deficit (LLD) has been evaluated in AMD
79 patients and is seen to be predictive of both the development of GA with subsequent visual
80 acuity loss and response to anti-VEGF treatment in neovascular AMD patients ^{11; 12}.

81 Here we report the first genome-wide investigation into genetic determinants for low-
82 luminance dysfunction in neovascular AMD utilizing patient data from the HARBOR clinical
83 trial¹³. The HARBOR trial was a dosing study which sought to determine the efficacy and safety
84 of 2.0 mg and 0.5 mg doses of ranibizumab (anti-VEGF antibody) in treatment naive patients
85 with choroidal neovascularization (CNV) secondary to AMD^{13; 14}. This study enrolled 1098
86 patients and followed them for one year. All dosing groups demonstrated clinically meaningful
87 visual improvement. Multiple clinical datapoints were collected at baseline, including LLD. We
88 separated the HARBOR patients into two groups for comparison, those with the largest LLD
89 differential (biggest drop in vision under low-luminance, quartile 4 = Q4) and those with the
90 smallest LLD differential before ranibizumab treatment (quartile 1 = Q1). We selected
91 phenotypic extremities instead of the whole patient population for two main reasons; (1) the
92 data looking at the effect of baseline LLD on anti-VEGF treatment response showed the largest
93 difference between Q1 and Q4 patients¹² and (2) it has been suggested as a way to increase
94 power in genetic studies¹⁵. Because the genetic underpinnings of LLD differential has not been
95 fully explored, we entered the study with the goal of identifying genetic factors involved in
96 LLD using common and rare variation assayed via whole genome sequencing (WGS) with
97 functional follow-up of biologically interesting hits. For functional characterization, we then

98 selected from the top hits the *CIDEA* gene as a compelling candidate gene with reported
99 function related to lipid metabolism, a pathway identified in previous AMD genetic analyses⁹.

100

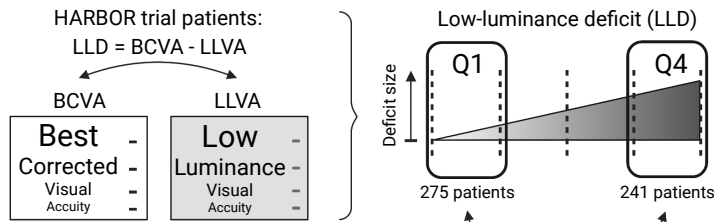
101

102 **Results**

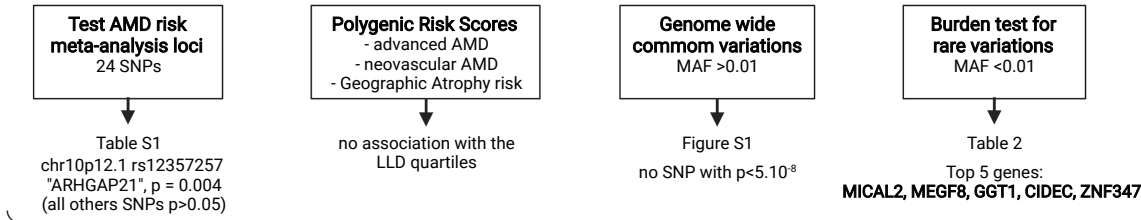
103 **A genome wide burden test identifies rare genetic variants in the *CIDEA* gene that are** 104 **enriched in AMD patients with small low-luminance deficit**

105 For our study, we subset the HARBOR ranibizumab dosing study population as
106 previously described for baseline low-luminance deficit (LLD)¹². All patients in the HARBOR
107 trial had neovascular AMD. This subsetting resulted in 275 patients in our Q1 group, and 241
108 patients in Q4 (**Figure 1A**). Detailed population characteristics are seen in **Table 1**. We
109 compared LLD quartiles 1 (Q1) and 4 (Q4) for this analysis, with the goal of maximizing the
110 phenotypic difference as seen in the previous anti-VEGF treatment response study¹². Patients
111 in Q1 (smallest low-luminance deficit) were seen to have better outcome on anti-VEGF therapy,
112 and slower visual acuity loss in GA patients than patients in Q4 (large low-luminance deficit)
113 ^{11; 12}. In our study population, patients in Q1 were more likely to have lower baseline visual
114 acuity, smaller baseline CNV leakage area, thinner sub-retinal fluid and a thinner choroid, but
115 did not significantly differ by age or sex (**Table 1**). We coded Q1 as the “cases” and Q4 as the
116 “controls”, so subsequently an odds ratio (OR)>1 indicates the minor allele was enriched in Q1
117 and an OR <1 indicates the minor allele was enriched in Q4.

A. Patient stratification

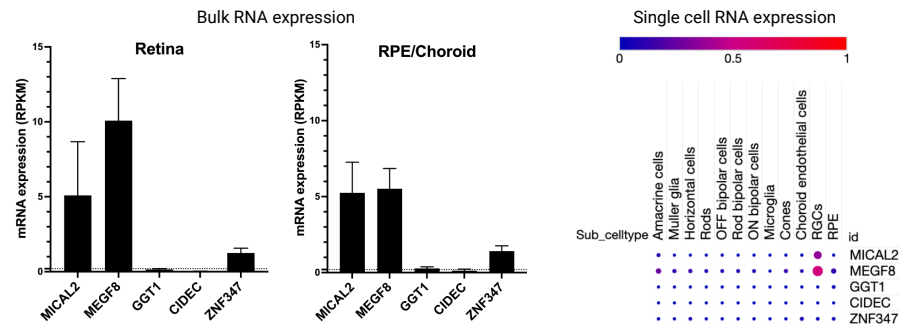


B. Genetic analysis



C. Gene prioritization for functional follow-up

| | Biological function | Mutation associated with disease reported (OMIM)? | Mostly expressed in? | Expressed in the eye? | Causal gene in the locus? | RV associated with Q1? | Biological pathway associated with AMD? | Biomarker opportunity? |
|----------------------------------|------------------------------------------|---------------------------------------------------|----------------------|-----------------------|---------------------------|------------------------|-----------------------------------------|------------------------|
| chr10p12.1 rs12357257 "ARHGAP21" | N/A | no | N/A | N/A | unknown | N/A | N/A | no |
| MICAL2 | F-actin disassembly protein | no | Brain, Artery | yes (RGCs) | yes, coding variants | yes | no | unlikely |
| MEGF8 | negative regulator of Hedgehog signaling | yes, AR, Carpenter syndrome (OMIM 614976) | Brain | yes (RGCs) | yes, coding variants | yes | no | unlikely |
| GGT1 | cysteinylglutathione homeostasis | yes, AR, Glutathionuria (OMIM 231950) | Kidney, Liver | very low | yes, coding variants | yes | no | yes |
| CIDECC | lipid metabolism | yes, AR, FPLD5 (OMIM 615238) | Adipose tissue | no | yes, coding variants | yes | yes | yes |
| ZNF347 | transcriptional regulation (?) | no | Brain | low | yes, coding variants | no | no | unlikely |



118 **Figure 1: Overview of the patient stratification, the lines of genetic investigation**
 119 **performed and the strategy used to prioritize genes for functional follow-up.**

120 (A). HARBOR patients were separated at baseline into two groups based on the size of their Low-
 121 Luminance Deficit (LLD): patients in quartile 1 (Q1) had the smallest drop in vision under low-
 122 luminance and patients in quartile 4 (Q4) had the biggest deficit. (B). Lines of genetic investigation and
 123 top-line results. (C) For functional analysis follow-up, top genetic hits were prioritized based on different
 124 criteria such as being the causal gene at the locus (presence of coding variants), the rare variants (RV)
 125 identified being enriched in Q1 patients, the gene playing a role in a biological pathway associated with
 126 AMD pathophysiology, and providing a potential biomarker opportunity. For the top hits, gene
 127 expression in human retina or RPE/choroid (bulk RNA sequencing, data from Orozco et al.³⁴) and in
 128 different human ocular cell types (single cell RNA sequencing, data from Gautam et al.³⁵) were also
 129 analyzed. AR: autosomal recessive; FPLD5: Familial Partial Lipodystrophy type 5. RGCs: Retinal
 130 Ganglion Cells. RPE: Retinal Pigment Epithelium.

| | Q1 | Q4 | p value | Missing (N%) | |
|--------------------------------------|--------------|--------------|----------|--------------|-----------|
| | | | | Q1 | Q4 |
| N | 275 | 241 | | | |
| Age | 78.61 (9.07) | 78.85 (7.94) | 0.75 | 0 (0%) | 0 (0%) |
| Female, N (%) | 117 (43%) | 105 (44%) | 0.81 | 0 (0%) | 0 (0%) |
| Baseline visual acuity | 48.0 (14.4) | 57.6 (9.2) | 5.12E-15 | 0 (0%) | 0 (0%) |
| Baseline CNV leakage area | 2.98 (1.83) | 4.35 (2.25) | 9.53E-12 | 0 (0%) | 0 (0%) |
| Baseline sub-retinal fluid thickness | 98 (95) | 172 (125) | 1.09E-11 | 0 (0%) | 0 (0%) |
| Baseline choroidal thickness | 174 (58) | 200 (77) | 0.0023 | 116 (42.2%) | 111 (46%) |

131 **Table 1.** Quartile Q1 and quartile Q4 AMD patient demographic comparison.

132

133 The lines of genetic investigation are outlined in **Figure 1B**. We first investigated the
134 loci identified in a recent AMD risk meta-analysis from the International AMD Genetics
135 Consortium (IAMDGC) (**Table S1**)⁸. After quality control procedures, 24 single-nucleotide
136 polymorphisms (SNPs) identified in the IAMDGC study were available for analysis. No locus
137 retained statistical significance after multiple testing. Two loci had $P < 0.1$, (1) *ARHGAP21*,
138 rs12357257, (odds ratio (OR) = 0.63, $p = 0.004$) and (2) *LIPC*, rs2043085, (OR = 1.29, $P = 0.10$).
139 We also constructed polygenic risk scores (PRS) for 1) advanced AMD risk 2) neovascular
140 AMD risk and 3) geographic atrophy risk from the same IAMDGC consortium analysis. We
141 did not find any of these PRS to be associated with our LLD population. Next, we examined
142 common variation throughout the genome (SNPs with a minor allele frequency (MAF) > 0.01).
143 There were no SNP which met the genome-wide significance level of $p < 5 \times 10^{-8}$ (**Figure S1**).

144 We then evaluated rare variation (SNPs with a $MAF < 0.01$) in the form of a burden test.
145 We included exonic SNPs predicted to have a moderate (e.g. amino acid changing) to high (e.g.
146 stop codon gain or loss) impact on the final protein sequence. No loci identified in the recent
147 GWAS meta-analysis were significantly associated in our burden test (all $p > 0.05$). No gene
148 burden test passed a Bonferroni multiple testing cutoff for the number of genes in the genome
149 tested. The top hits for this analysis are presented in **Table 2**.

| Gene | Q1 Freq | Q4 Freq | # SNPs | OR | p value |
|---------------|---------|---------|--------|------|----------|
| <i>MICAL2</i> | 0.14 | 0.06 | 28 | 3.38 | 0.00077 |
| <i>MEGF8</i> | 0.12 | 0.05 | 27 | 3.75 | 0.000977 |
| <i>GGT1</i> | 0.16 | 0.08 | 24 | 2.88 | 0.001055 |
| <i>CIDEA</i> | 0.06 | 0.02 | 5 | 7.14 | 0.001076 |
| <i>ZNF347</i> | 0.02 | 0.10 | 15 | 0.20 | 0.001679 |

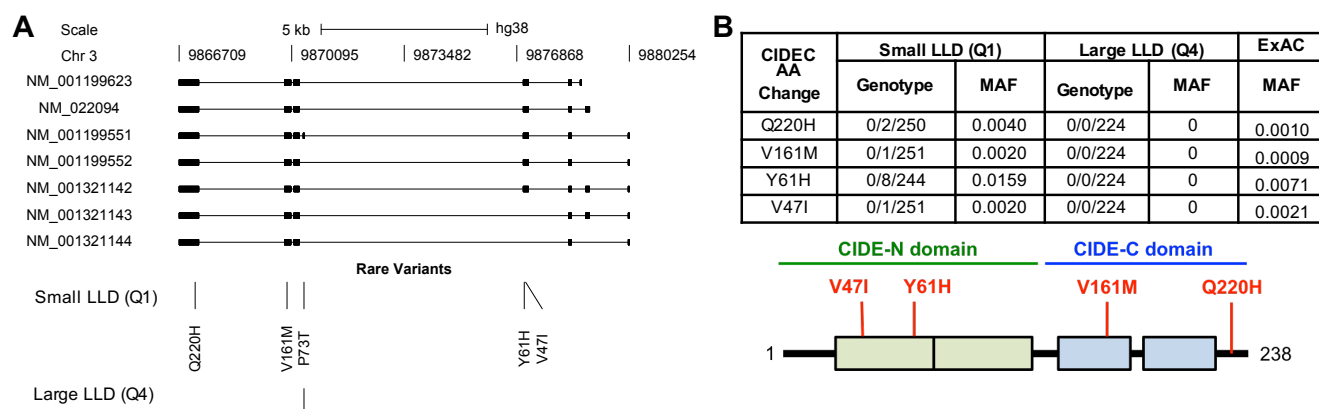
150 **Table 2.** Results from rare variant burden test comparing quartile Q1 and quartile Q4 AMD
151 patients. OR = odds ratio.
152

153 For functional analysis follow-up, we prioritized the top genetic hits identified by our
154 common and rare variants analysis using different criteria (**Figure 1C**). We decided to select
155 *CIDEA* for a thorough wet lab analysis as it was the probable causal gene at the identified locus
156 (presence of coding variants), the rare variants identified were enriched in Q1 patients (i.e.
157 associated with better outcome). Furthermore, *CIDEA* is involved in a biological pathway
158 already associated with AMD (i.e. lipid metabolism) and since *CIDEA* expression is broad in
159 the human body (adipose tissue), it provides a potential biomarker opportunity¹⁶, which is
160 usually not the case when the gene expression is restricted to the neuroretina.

161 The *CIDEA* gene encodes the *CIDEA* protein (NP_001365420.1; OMIM: 612120), a
162 member of the Cell-death-Inducing DNA fragmentation factor (DFF)45-like Effector (*CIDE*)
163 family. As this is the first report of *CIDEA* affecting AMD pathology, we looked for evidence
164 of *CIDEA* rare variant involvement in the UK Biobank sequencing data via the GENEASS
165 portal (v0.7.8alpha)¹⁷. We did not see evidence of a strong phenotype associated with rare
166 variants in *CIDEA* with regards to any distinct ocular phenotype, with “eye problems/disorders”
167 being the top ocular phenotype in the pLoF analysis (**Table S2**; P=0.005).

168 The *CIDEA* rare alleles found in our analysis were found in 6% of Q1 patients and
169 spread over multiple exons. In the Q4 patients, rare alleles were found in 2% of individuals and
170 they coalesced to one exon seen only in RefSeq transcript NM_001199551 (**Figure 2A**). We
171 sought to quantify the percentage of transcripts expressed that are NM_001199551 in the GTEx

172 database for adipose tissue and blood ¹⁸. In both sample types, percent expression of
 173 NM_001199551 was 0.5% of all *CIDE*C transcripts (**Figure S2 – adipose pictured, blood**
 174 **similar**). In conclusion, if restricting the analysis in *CIDE*C to exons contained in transcripts
 175 that are more widely expressed we found that *CIDE*C rare variation was exclusive to the Q1
 176 AMD patients (N=12). The four SNPs identified in Q1 patients were rs150971509 c.139G>A
 177 [p.Val47Ile], rs79419480 c.181T>C [p.Tyr61His], rs145323356 c.481G>A [p.Val161Met] and
 178 rs52790883 c.660G>T [p.Gln220His] (subsequently referred to as V47I, Y61H, V161M and
 179 Q220H respectively) (**Figure 2B**). We used the software PolyPhen-2 (Polymorphism
 180 Phenotyping v2) to perform *in silico* prediction of the possible impact of these four amino acid
 181 substitutions on *CIDE*C stability or function ¹⁹. The V47I substitution was predicted as probably
 182 damaging, the V161M and Q220H substitutions were predicted as possibly damaging and only
 183 the Y61H substitution was predicted to be benign. Since no structural data was available for the
 184 full *CIDE*C protein, these predictions were based solely on evolutionary comparisons. Thus,
 185 we decided to include all four rare variants identified in our Q1 AMD *CIDE*C patients in our
 186 experimental follow-up.



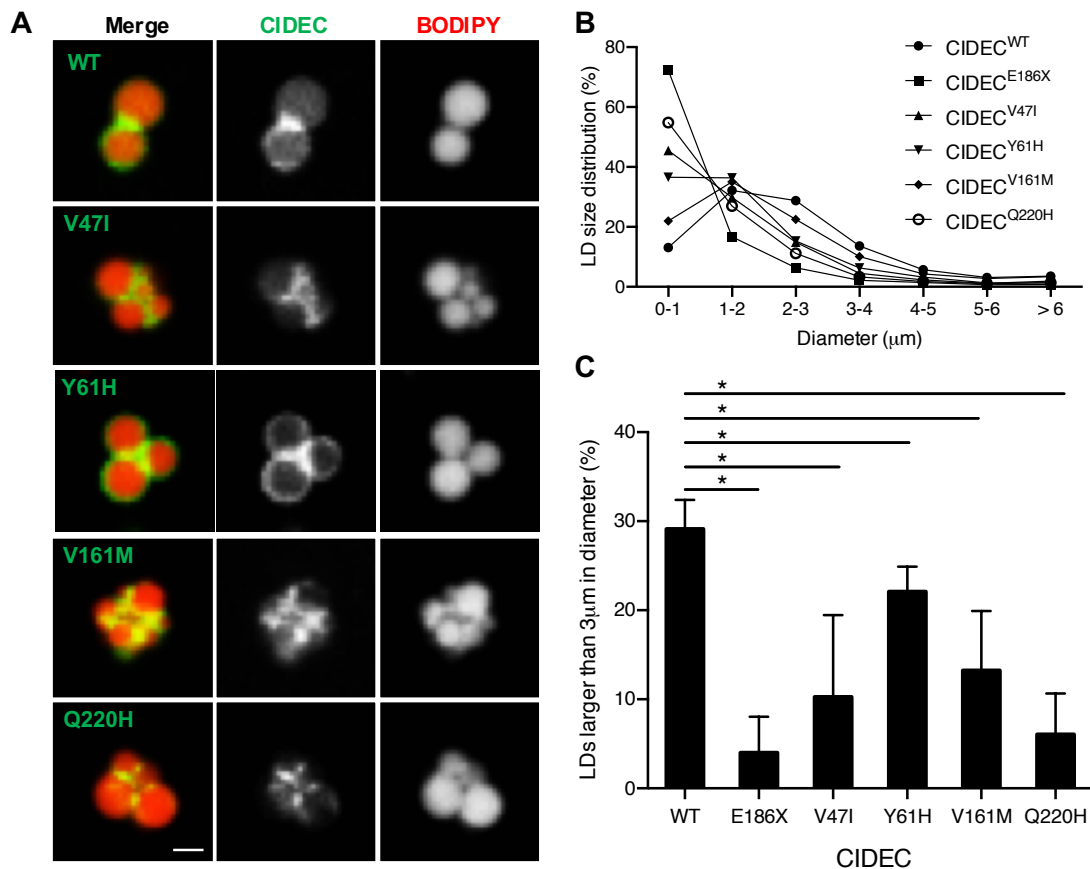
187 **Figure 2. Genetic analysis of low-luminance deficit quartile Q1 and quartile Q4 AMD patients.**
 188 (A) Genetic diagram of *CIDE*C and location of rare variants in Q1 and Q4 AMD patients. SNPs are
 189 indicated by amino acid change and position. (B) Table of genotype and minor allele frequencies for
 190 variants selected for further analysis and map of *CIDE*C protein with CIDE-N and CIDE-C domains
 191 with these SNPs annotated by position and amino acid change.
 192

193 **Q1 AMD CIDEC rare alleles cause a defect in lipid droplet fusion and enlargement.**

194 *CIDEC* is a homolog of the murine *Fsp27* (Fat-specific protein 27kDa) gene²⁰. *Fsp27*
195 was originally identified as a gene up-regulated during murine pre-adipocytes differentiation *in*
196 *vitro*^{21; 22}. FSP27 was then shown to localize to lipid droplets (LDs) in adipocytes, where it
197 promotes triglyceride storage by inhibiting LD fragmentation and lipolysis²³. *In vivo*, FSP27
198 is mainly expressed in the white adipocytes where it contributes to optimal energy storage by
199 allowing the formation of their characteristic large unilocular LD²⁴. *Fsp27* deficient mice have
200 white adipocytes with small multilocular LDs and increased mitochondrial size and activity,
201 resulting in smaller white fat pads and increased metabolic rate^{24; 25}. A *CIDEC* homozygous
202 nonsense mutation was identified in a patient with partial lipodystrophy and insulin resistant
203 diabetes (OMIM: 615238)²⁶. This p.Glu186* (E186X, c.556G → T) mutation results in
204 truncation of the *CIDEC* protein and the patient presented with multilocular small LDs and
205 focal increased mitochondria density in adipocytes. Notably, *Fsp27* deficient mice have a
206 healthy metabolic profile but when challenged by substantial energetic stress, they acquire
207 features found in the *CIDEC* E186X patient, such as insulin resistance and hepatic steatosis²⁷.
208 However, no eye phenotype has been reported in the *CIDEC* E186X patient nor the *Fsp27*
209 deficient mice. Therefore, we first investigated the potential functional consequences of the
210 four rare, protein altering *CIDEC* alleles found in Q1 AMD patients in adipocytes, a cell type
211 in which *CIDEC*'s function has been well established.

212 First, we transiently expressed different versions of *CIDEC* tagged with GFP into 3T3-
213 L1 pre-adipocytes. We transfected each of the four Q1 AMD rare variants (V47I, Y61H,
214 V161M and Q220H) and as controls, we transfected cells with *CIDEC* wild-type (WT) or with
215 the *CIDEC* E168X mutation. Subsequently, the proteins encoded by the Q1AMD rare *CIDEC*
216 alleles will be referred to as “AMD *CIDEC* variants”. The cells were then treated for two days

217 with oleic acid to induce LD formation. As expected, the mutant CIDEC E168X was diffused
 218 in the cytoplasm and failed to accumulate around the LDs (data not shown, and ²⁶). In contrast,
 219 the four AMD CIDEC variants mostly localized to LDs in transfected adipocytes, and similarly
 220 to CIDEC WT, accumulated at the LD-LD contact sites (**Figure 3A**).
 221



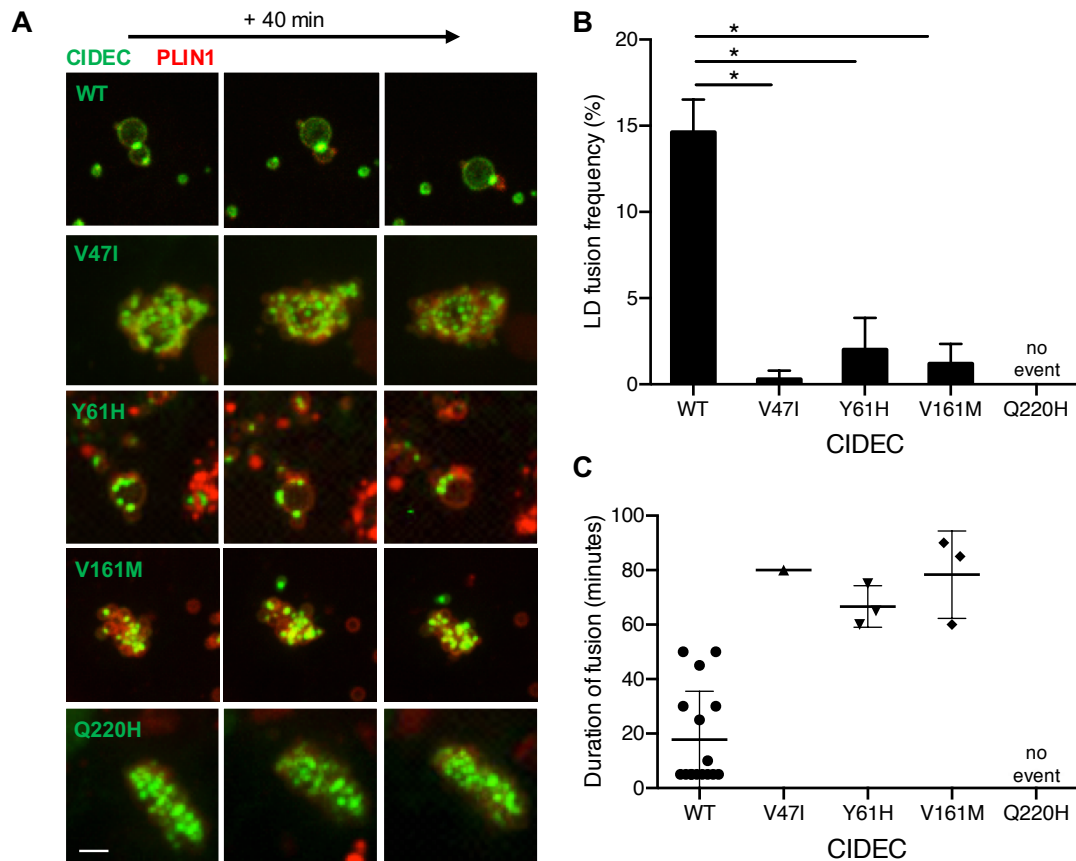
222 **Figure 3. AMD CIDEC variants localize to lipid droplets (LDs) but cause a defect in LD**
 223 **enlargement.** (A) Representative images of GFP-tagged CIDEC wild-type (WT) or rare variants
 224 localized to LDs labeled in red by BODIPY 558/568. Scale bar: 2 μm. (B) Size distribution of LDs in
 225 pre-adipocytes expressing CIDEC WT or each of the rare variants (diameters in μm). (C) Percentage of
 226 LDs with a diameter larger than 3 μm. N=3 (mean ± SD, Student's t test, *p<0.05)
 227

228 Next, we assessed the size of the LDs in the transfected adipocytes. We found that cells
 229 transfected with CIDEC WT had LDs with an average diameter of 2 to 3 μm. However, cells
 230 expressing CIDEC E168X had a severe LD enlargement defect, resulting in accumulation of
 231 clustered LDs with diameters smaller than 1 μm. Cells expressing each of the AMD CIDEC

232 variants had an intermediate phenotype with a majority of LDs being smaller than 2 μm
233 (**Figures 3B and C**). Interestingly, unlike in the E168X mutation case or *Fsp27* deficiency, we
234 found that the presence of the AMD CIDEc variants did not increase the density of
235 mitochondria in the transfected cells (**Figure S3A**) and they did not alter mitochondria activity
236 as measured with a Seahorse bioanalyzer (**Figure S3B**). In conclusion, the AMD CIDEc
237 variants do not impair proper CIDEc localization to LDs and do not increase mitochondrial
238 density, but they are hypomorphic variants reducing the LD enlargement capacity in adipocytes.

239 Next, we transiently co-expressed GFP-tagged version of CIDEc WT or each of the
240 four AMD CIDEc variants with mCherry-tagged Perilipin1 (PLIN1) in 3T3-L1 pre-adipocytes.
241 PLIN1 is an adipocyte-specific LD-associated protein that interacts with and potentiates the
242 function of murine CIDEc and hence could be used to track individual LDs²⁸. After inducing
243 LD formation with oleic acid treatment, we performed time-lapse imaging over 6 hours to
244 quantify the number of LD fusion events (**Figure 4 and Video 1**). Cells expressing each of the
245 AMD CIDEc variants showed significant defects in LD fusion frequency compared to cells
246 expressing CIDEc WT (Student's t-test, $p < 0.005$). Over 6 hours, cells expressing CIDEc WT
247 had $14.6\% \pm 1.9\%$ of their LDs achieving fusion (**Figures 4A and B**). Cells expressing CIDEc
248 V47I, Y61H and V161M had a severe decrease in LD fusion events with only $0.3\% \pm 0.5\%$,
249 $2.0\% \pm 1.8\%$ and $1.2\% \pm 1.1\%$ of LDs achieving fusion respectively. No LD fusion events were
250 recorded during the 6 hours in cells expressing CIDEc Q220H, suggesting that this variant
251 causes a severe loss of LD fusion capacity. Quantification of the time required from initial
252 contact to complete fusion of two LDs revealed that LD fusion events slowdown in presence of
253 the CIDEc variants (**Figure 4C**). In conclusion, adipocytes expressing the AMD CIDEc
254 variants have a defect in LD fusion capacity, with merging events being slower and rarer than
255 the ones occurring in cells expressing CIDEc WT.

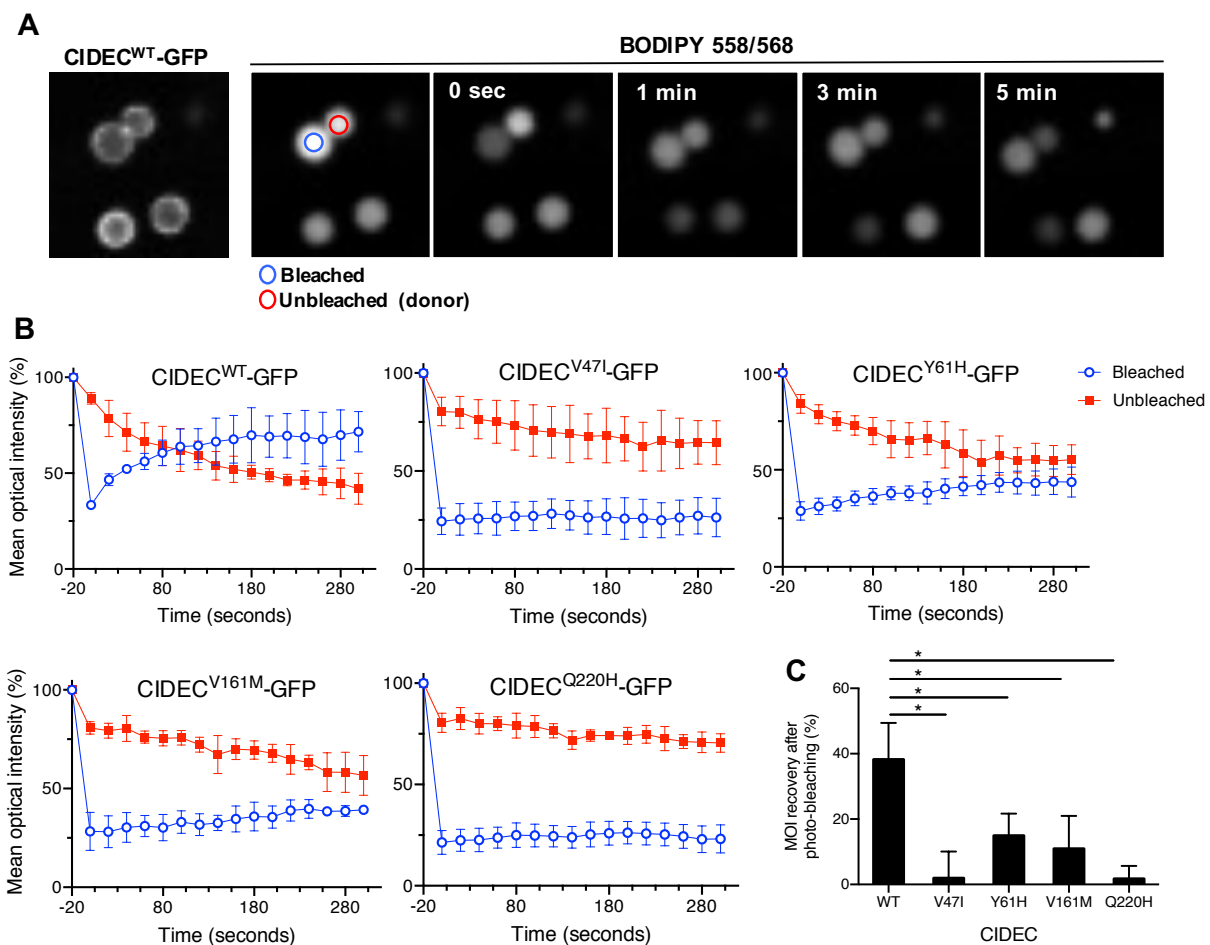
256



257 **Figure 4. Lipid droplet (LD) fusion occurs less frequently and more slowly in pre-adipocytes**
258 **expressing the AMD CIDECC rare variants.** (A) Representative time-lapse images over 40 minutes of
259 LDs in cells co-expressing GFP-tagged CIDECC WT (taken from **Video 1**) or each of the rare variants,
260 and mCherry-tagged PLIN1. Scale bar: 2 μ m. (B) Percentage of LDs undergoing fusion during the 6-
261 hour analysis. N=3 (mean \pm SD, Student's t test, * p <0.05). (C) Time in minutes required from initial
262 LD-LD contact to complete LD fusion.
263

264 Finally, we performed a Fluorescence Recovery After Photobleaching (FRAP)
265 experiment to determine if the CIDECC variants could affect the kinetics of lipid diffusion
266 between LDs. We transiently transfected 3T3-L1 pre-adipocytes with GFP-tagged CIDECC WT
267 or AMD variants, induced LD formation and labeled LDs with the fluorescent fatty acid
268 BODIPY 558/568 dye. Focusing on adjoining LDs of equivalent size and expressing CIDECC at
269 the contact site, we photobleached one LD and measured the mean optical intensity (MOI) of
270 both the bleached and the neighboring, unbleached LD. Recovery of fluorescence on the
271 bleached LD over time was used to quantify the rate of lipid exchange between the two LDs
272 (**Figure 5A**). In cells expressing CIDECC WT, the fluorescence recovered to about 75% of the

273 pre-bleach intensity within 3 minutes in the photobleached LD. This recovery was accompanied
 274 by a corresponding decrease in fluorescence on the unbleached LD, reflecting efficient lipid
 275 exchange between the two LDs (**Figures 5B and C**). In cells expressing CIDEC Y61H or
 276 V161M, fluorescence recovery in the bleached LD exhibited a delayed and reduced
 277 fluorescence compared to cells expressing CIDEC WT. In cells expressing CIDEC V47I or
 278 Q220H there was very limited, if any, fluorescence recovery on the bleached LD, suggesting
 279 loss of lipid exchange capacity (**Figures 5B and C**). In conclusion, the presence of the AMD
 280 CIDEC variants impairs the lipid diffusion capacity between LDs in adipocytes.



281 **Figure 5. AMD CIDEC variants cause a decrease in the lipid exchange rate between lipid droplets**
 282 **(LDs).** (A) Representative Fluorescence Recovery After Photobleach (FRAP) images of paired LD
 283 expressing GFP-tagged CIDEC wild-type (WT) showing progressive neutral lipid (BODIPY 558/568
 284 dye labeling) exchange as determined by fluorescence recovery from the adjacent LD. (B)
 285 Quantification of mean optical intensity (MOI) in the bleached (blue circle) and unbleached (red circle)
 286 LD in cells expressing CIDEC WT or each of the rare variants. (C) Percentage of MOI recovery on
 287 bleached LDs from 0 sec. to 300 seconds. N=3 (mean \pm SD, Student's t test, * p <0.05).

288 Collectively, these results show that the AMD CIDEDEC variants do not affect CIDEDEC
289 localization to LD contact sites, but they impair the lipid exchange capacity between LDs,
290 resulting in defective LD fusion and incapacity for the adipocytes to accumulate lipids inside
291 few large LDs.

292

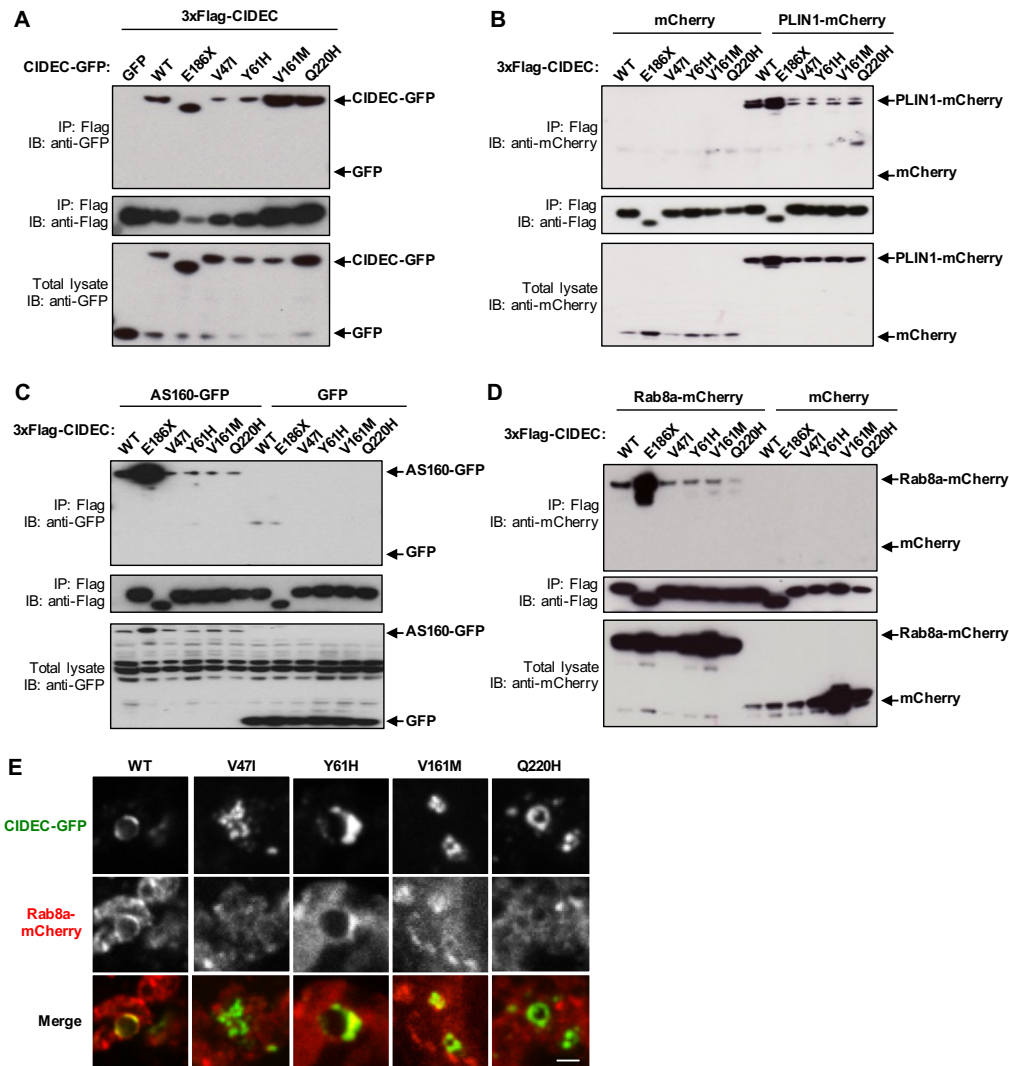
293 **Q1 AMD CIDEDEC rare alleles decrease the binding affinity of CIDEDEC with the lipid droplet**
294 **fusion effectors PLIN1, RAB8A and AS160.**

295 LDs are highly dynamic organelles containing a neutral lipid core enclosed in a
296 phospholipid monolayer decorated by a large number of proteins^{29;30}. To better understand the
297 functional consequences of the AMD CIDEDEC alleles and how they can affect LD fusion, we
298 examined if they could alter protein-protein interactions. Indeed, CIDEDEC-mediated LD fusion
299 is different from other membrane fusion events. CIDEDEC proteins need to first accumulate at the
300 contact site between two LDs, to then enable recruitment of regulator proteins such as PLIN1,
301 RAB8A and AS160, which facilitate the lipid transfer through the fusion pore³¹.

302 We first assessed if the variants affected CIDEDEC capacity to homodimerize. CIDEDEC
303 contains two conserved CIDE domains allowing its dimerization, a N-terminal CIDE-N domain
304 and a C-terminal CIDE-C domain^{(20; 32} and **Figure 2B**). The CIDE-N domain, in which the
305 variants V47I and Y61H are located, dimerizes mainly via electrostatic interactions, while the
306 CIDE-C domain that contains the V161M variant dimerizes through a stronger interaction²⁸.
307 Q1 AMD patients are heterozygous for the different CIDEDEC alleles, so HEK 293T cells were
308 co-transfected with 3xFlag-CIDEDEC WT and either CIDEDEC WT, the E186X mutation or one of
309 the AMD CIDEDEC variants tagged with GFP. After immunoprecipitation of the 3xFlag-CIDEDEC
310 WT, pulled-down proteins were probed with anti-GFP. Co-transfection of the 3xFlag-CIDEDEC
311 WT together with GFP alone served as negative control. The CIDE-N domain variants V47I

312 and Y61H showed decreased dimerization capacity with CIDEDEC WT, whereas the two other
 313 variants V161M and Q220H did not affect the binding ability (**Figure 6A**). The pathogenic
 314 mutation CIDEDEC E186X, located in the CIDE-C domain, also did not affect the binding affinity
 315 with CIDEDEC WT.

316



317 **Figure 6. AMD CIDEDEC variants in the CIDE-N domain decrease dimerization affinity and all four**
 318 **variants decrease binding to effector partners PLIN1, AS160 and RAB8A.** (A) 3xflag-tagged
 319 CIDEDEC wild-type (WT) was co-transfected with the indicated GFP-tagged CIDEDEC variants in HEK
 320 293T cells. GFP alone was used as negative control. 3xflag-tagged CIDEDEC WT was immuno-
 321 precipitated (IP) using anti-Flag and pulled-down proteins were immuno-blotted (IB) with anti-GFP and
 322 anti-Flag. Total cell lysate was immunoblotted with anti-GFP to control for CIDEDEC-GFP expression
 323 levels. (B-E) HEK 293T cells were co-transfected with 3xFlag-CIDEDEC WT, E186X or AMD variants,
 324 and either PLIN1-mCherry (B), AS160-GFP (C) or RAB8A-mCherry (D). After immunoprecipitation
 325 (IP) of the 3xFlag-CIDEDEC, pulled-down proteins were probed with anti-mCherry or anti-GFP, and anti-
 326 Flag. Co-transfection with mCherry or GFP alone was used as negative controls. Total cell lysates were
 327 immunoblotted (IB) with anti-mCherry or anti-GFP to control for PLIN1, AS160 and RAB8A
 328 expression levels. (E) Representative fluorescence images of 3T3-L1 pre-adipocytes lipid droplets
 329 containing CIDEDEC-GFP wild-type (WT) or variants and RAB8A-mCherry. Scale bar: 2 μm.

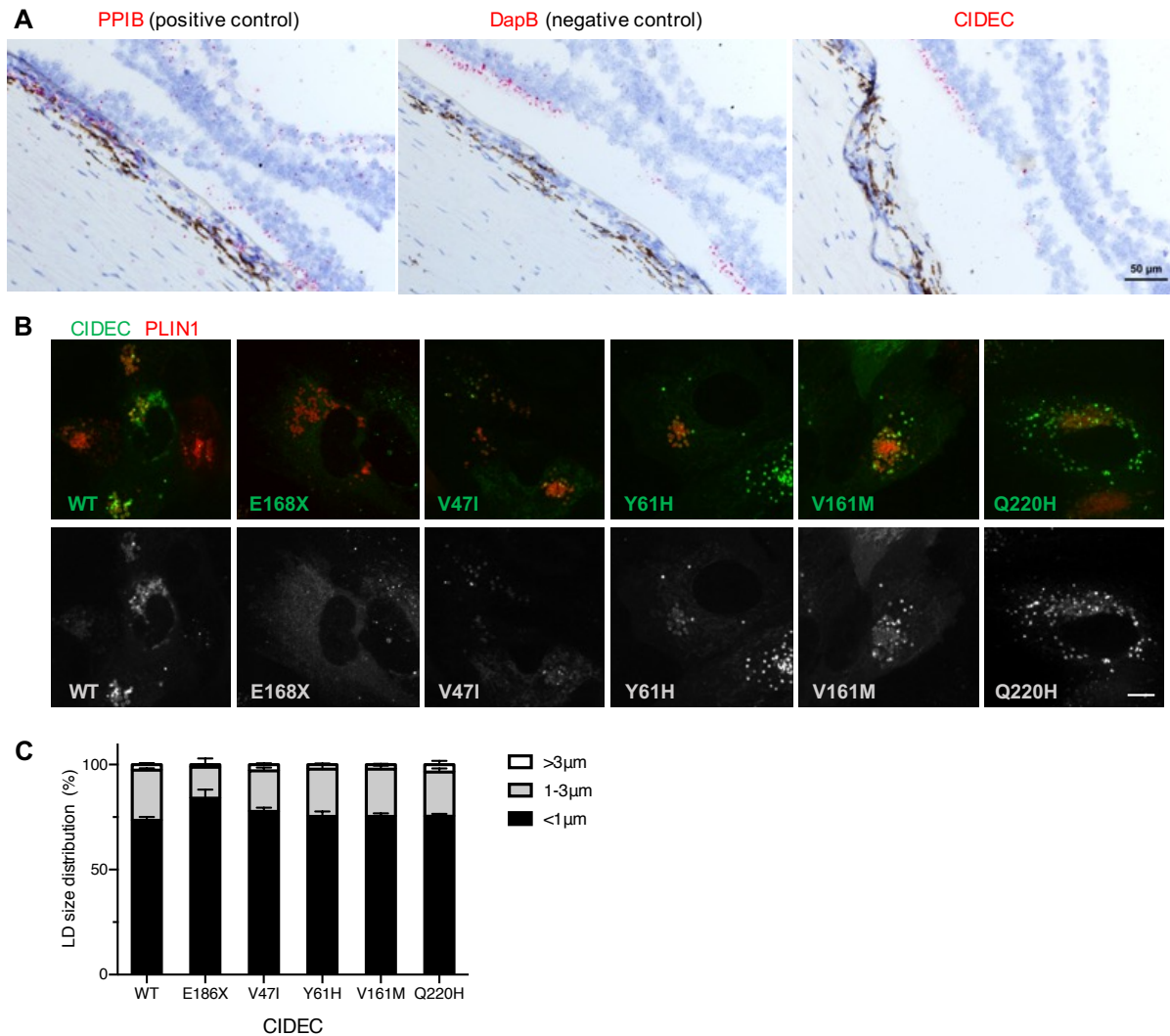
330 Next, we assessed if the AMD CIDEDEC variants affect CIDEDEC capacity to interact with
331 its LD-associated regulatory partners PLIN1, RAB8A and AS160, as these interactions are
332 required for LD fusion and growth^{28; 33}. We co-transfected HEK 293T cells with 3xFlag-
333 CIDEDEC WT, E186X or the AMD CIDEDEC variants, and either PLIN1-mCherry, AS160-GFP or
334 RAB8A-mCherry. After immunoprecipitation of the 3xFlag-CIDEDEC, pulled-down proteins
335 were probed with anti-mCherry or anti-GFP. Strikingly, all four AMD CIDEDEC variants had
336 similarly decreased binding affinity with PLIN1 (**Figure 6B**) and AS160 (**Figure 6C**). All four
337 AMD CIDEDEC variants also showed decreased binding capacity with RAB8A, however, the
338 Q220H variant caused a more severe loss of interaction with the GTPase (**Figure 6D**). Only a
339 fraction of RAB8A and AS160 are associated to LDs, with the rest being distributed in the
340 cytoplasm (**Figure 6E and Figure S4**). The fact that the E186X mutant is abnormally diffuse
341 in the cytoplasm could explain its stronger interaction with the binding partners compared to
342 CIDEDEC WT, which is concentrated on the LDs (**Figures 6B, C and D**).

343 Collectively, these results show that the AMD CIDEDEC variants V47I and Y61H, located
344 in the CIDE-N domain decrease CIDEDEC dimerization capacity and its binding ability with the
345 regulators partners PLIN1, RAB8A and AS160. The two other variants, V161M and Q220H,
346 which are not in the CIDE-N domain, do not affect CIDEDEC ability to dimerize, however, they
347 nevertheless also decrease its interaction with PLIN1, RAB8A and AS160. The reduced
348 interaction capacity of the four AMD CIDEDEC variants with its binding partners may explain
349 how their presence causes a defect in lipid droplet fusion and enlargement in adipocytes.

350

351 **CIDEDEC expression is not detected in the human retina or the Retinal Pigment Epithelium**
352 **and the Q1 AMD CIDEDEC variants do not affect the size of the retinosomes.**

353 CIDEDEC plays a critical role in the white adipose tissue, but is also expressed in organs
354 such as muscles, nerves and even blood vessels¹⁸. CIDEDEC expression in the eye has been
355 reported after an Expressed Sequence Tag (EST) database search, however, it is not known if
356 the expression comes from the neuroretina or the eye globe supportive tissue³². The key
357 elements of the eye involved in AMD are the photoreceptors, an epithelium located underneath
358 the retina called the Retinal Pigment Epithelium (RPE) and the blood vessels supporting the
359 retina called the choroid. To investigate the potential expression of *CIDEDEC* in these structures,
360 we first used published human RNA sequencing datasets. *CIDEDEC* was not detect in human
361 retina or RPE/choroid (bulk RNA sequencing³⁴) and in different human ocular cell types (single
362 cell RNA sequencing³⁵) (**Figure 1C**). To investigate further the potential expression of *CIDEDEC*
363 in the eye, we performed RNA *in situ* hybridization on eye sections from a Caucasian 73-year
364 old female and a Caucasian 88-year old male, both without history of AMD (**Figure 7A**). We
365 also performed *Fsp27* RNA *in situ* hybridization on mouse eye sections (**Figure S5**). In both
366 human and mouse eyes, we did not detect CIDEDEC RNA in the retina, the RPE or the choroid
367 (**Figure 7A and Figure S5**). We used the sensitive detection method BaseScope™ (Advanced
368 Cell Diagnostics (ACD)) and found that the signal detected with the CIDEDEC probes on the
369 human eye sections were consistent with the background signal detected using the bacterial
370 gene *DapB* as a negative control (**Figure 7A**). On the mouse eye sections, we found rare cells
371 positive for *Fsp27* expression but these cells were in the supportive tissue around the eye
372 (**Figure S5**).



373

374 **Figure 7. CIDEA RNA is not detected in the human eye and exogenous expression of the CIDEA**
375 **variants does not affect lipid droplets (LDs) size in Retinal Pigment Epithelium (RPE) cells. (A)**
376 **In situ hybridization in the fovea of a control human donor eye showing that CIDEA RNA is not detected**
377 **in the retina or RPE cells. Detection of PPIB (red) was used as positive control and detection of bacterial**
378 **DapB was used as negative control and evaluation of the non-specific background. Scale bar: 50 μm.**
379 **(B and C) Human fetal RPE cells were co-infected with lentivirus expressing CIDEA variants and**
380 **PLIN1 as marker for LDs. The infected cells were differentiated for 3 weeks before oleic acid**
381 **stimulation. Representative images of RPE cells expressing both CIDEA variants and PLIN1 (B). LD**
382 **diameters were quantified by diameter range as depicted in the bar graph (n=3; mean ± SD) (C). Scale**
383 **bar: 5 μm.**
384

385 RPE cells contain specific LDs called retinosomes, in which retinyl esters are stored and
386 used to replenish key components of the visual cycle^{36; 37}. To account for the possibility that
387 CIDEA was expressed below our detection threshold in RPE cells, we tested if exogenous AMD
388 CIDEA variants could have consequences on the size of these specialized LDs, retinosomes.

389 Primary human fetal RPE cells were infected with lentivirus encoding CIDEA WT or the AMD
390 CIDEA variants and differentiated for three weeks before oleic acid stimulation and LD
391 labelling. Similar to the localization in adipocytes, CIDEA WT and AMD CIDEA variants
392 accumulate on retinosomes and concentrate at the LD fusion sites in RPE cells (**Figure 7B**).
393 However, the RPE cells failed to form large LDs after oleic acid stimulation and the majority
394 of the retinosomes in RPE cells expressing CIDEA WT were smaller than 1 μm in diameter
395 (**Figure 7C**). Consequently, we did not observe any difference in LD size between the RPE
396 cells expressing the CIDEA WT and the cells expressing the different AMD CIDEA variants.

397 Finally, we compared color fundus photos (**Figure 8**) and Optical Coherence
398 Tomography (OCT) images (not shown) from the eyes of the Q1 AMD CIDEA variant carriers
399 and Q1 AMD CIDEA variant non-carriers. In particular, we wanted to know if by disrupting
400 lipid accumulation, the CIDEA variants could affect size and accumulation of drusen, which
401 are deposits of proteins and lipids building up under the retina and a hallmark of AMD.
402 However, we did not observe unique ocular clinical features in patients carrying the CIDEA
403 rare variants (**Figure 8B**) compared to non-carriers (**Figure 8A**). In both groups, we observed
404 typical AMD clinical features such as pigmentary changes, variable amount of drusen,
405 geographic atrophy and choroidal neovascular lesions.

406 In conclusion, we did not detect CIDEA expression in the ocular structures directly
407 affected in AMD. We also found that exogenous expression of the AMD CIDEA variants did
408 not alter retinosome size in RPE cells, and that AMD patients carrying the CIDEA variants do
409 not present unique phenotypic ocular features compared to non-carriers. Our results suggest
410 that the AMD CIDEA variants do not play a direct role in the eye. Additional experiments using
411 conditional mouse models will be important to assigning the tissue specific effects of CIDEA
412 variants and the role of LD dysregulation in AMD.



413
414
415
416
417
418
419

Figure 8. Clinical images of patients in the low-luminance deficit quartile Q1. Color fundus photos (CFP) from participants in the HARBOR trial (A) Q1 non-carriers for CIDECD rare variants (B) Q1 rare variant CIDECD carriers. CFP in both groups demonstrate typical clinical features of macular degeneration such as pigmentary changes, drusen, geographic atrophy and choroidal neovascular lesions. No obvious phenotypic differences are noted between the two groups.

420 Discussion

421 Here we report the first analysis examining the genetic effect on baseline LLD, a clinical
422 measurement that has been shown to be predictive of anti-VEGF treatment response and GA
423 lesion growth, in AMD patients. While the study is of modest size, to our knowledge, it is novel
424 in its effort to utilize clinical indices beyond BCVA that have been linked to patient outcomes
425 to further homogenize AMD patients in order to increase power for genetic analysis. It is our
426 hope that as datasets increase in size and have deeper phenotypic assessment, these types of
427 sub-phenotype GWAS analyses will increase and work alongside recent studies utilizing novel
428 *in vitro* methods, such as those described here and genome-wide single cell and perturbation
429 methods to help uncover the functionality of genes associated with the pathogenesis of AMD.

430 We did not find any variants, either in the common or the rare variant burden analysis
431 which passed a pre-specified significance threshold accounting for multiple testing. This can

432 occur for several reasons. One reason could be that the effect of patient germline genetics is
433 not substantial on low-luminance visual acuity and that environmental factors explain more of
434 the risk variability. Another is that we are underpowered for a genome wide analysis in our
435 study population. As such, it will be important to replicate the genetic findings in a secondary
436 cohort which has similar phenotyping and sequencing data. Since all patients in our analysis
437 are advanced AMD patients, and *CIDEC* has not been reported previously as an AMD risk
438 gene, this could indicate that *CIDEC* rare variants play a role only once a patient develops
439 advanced disease. Datasets with deep phenotyping of advanced AMD patients would be
440 required for replication. While large scale biobank data exist (e.g. U.K. BioBank), and are
441 exceptionally useful for most replication analyses, these datasets do not currently have the
442 ability to delve deep into clinical features for an age-related disease such as AMD. Conversely,
443 smaller, more phenotypically focused genetic datasets such as the one used in this study are
444 useful for identification of signals and hypotheses, but are severely underpowered to confirm
445 an association statistically. As such, we sought to assess the possible contribution of *CIDEC*, a
446 gene with biology tangential to genes in known AMD risk loci, to AMD pathology through *in*
447 *vitro* analysis.

448 In our rare variant burden analysis, we noticed that one of the top hits was strongly
449 linked with lipid metabolism. Similarly, multiple loci identified in AMD risk studies contain
450 genes implicating lipid metabolism. Due to sample size constraints, and the low frequency of
451 *CIDEC* variants, we were unable to test for interaction between known AMD risk alleles and
452 the *CIDEC* variants. Rare, protein altering variants were enriched in the patients with small
453 LLD. Previous studies associated a small LLD at baseline with more favorable prognostic and
454 predictive outcomes. Thus, possible impairment of *CIDEC* function could be beneficial for

455 AMD patients and we undertook characterization of the *CIDEC* variants in further studies,
456 which focused on the exact variants seen in our AMD cases.

457 In our *in vitro* analysis, we interestingly found that all four rare variants failed to impair
458 *CIDEC* localization to LDs, but instead all decreased the binding affinity of *CIDEC* with the
459 LD fusion effectors *PLIN1*, *RAB8A* and *AS160*. Interaction of *CIDEC* with these binding
460 partners is critical for its function and we hypothesize that this decreased interaction underlies
461 the defect in LD enlargement and lipid exchange that we observed in adipocytes expressing the
462 AMD *CIDEC* variants. Interestingly, the functional consequences that we uncovered are milder
463 than the ones caused by the lipodystrophic E168X variant and are restricted to the LD capacity
464 to fuse and increase lipid storage. Indeed, the AMD *CIDEC* variants are hypomorphic regarding
465 LD size and they do not affect mitochondria density or activity. Our data suggest that the Q1
466 AMD *CIDEC* variants do not severely disrupt adipocyte health and function and may have a
467 beneficial effect by only limiting the capacity of adipocytes to accumulate lipids in very large
468 LDs.

469 Of note, patients carrying the Q1 AMD *CIDEC* variants are heterozygotes, contrasting
470 with the E168X homozygote lipodystrophic patient. Furthermore, heterozygous *Fsp27* wt/ko
471 mice have normal weight and the appearance of their adipose tissue is similar to the one from
472 *Fsp27* wt/wt mice²⁴. Thus, it is likely that the Q1 AMD *CIDEC* patients did not suffer from
473 severe lipodystrophy and that they only had sub-clinical consequences of the *CIDEC* variants
474 expression. Our results suggest that *CIDEC* is not expressed in the ocular tissue affected in
475 AMD such as the retina, RPE and choroid. This points out toward a “systemic” effect of the
476 beneficial Q1 AMD *CIDEC* variants. Interestingly, a similar indirect and systemic favorable
477 effect has recently been reported in mouse models of vascular inflammation and atherogenesis
478 after *Fsp27* silencing^{38; 39}. Many studies on dietary or circulating lipids, as well as genetic

479 studies support a role for not only local lipid trafficking in the retina but also for circulating
480 lipoproteins in AMD pathogenesis⁴⁰. Therefore, it would have been interesting to perform a
481 biomarker investigation of the HARBOR patient serum to know if any particular change(s) in
482 circulating lipoproteins levels could be detected in patients carrying the Q1 AMD CIDEA
483 variants compared to non-carriers (unfortunately, such samples were not available for us to
484 perform the analysis). In addition to lipoproteins, it would also have been interesting to probe
485 the AMD patient serums for changes in adipokines, the cytokines secreted by adipocytes.
486 Indeed, it has been shown that hypertrophied adipocytes can lead to local inflammation and
487 inhibition of production of adipokines, such as adiponectin⁴¹. Since adipocytes expressing the
488 AMD CIDEA variants have a decreased LD enlargement capacity, it may prevent them from
489 becoming hypertrophic, keeping adiponectin level high. Supporting this idea, it has been
490 reported that the *Fsp27* deficient mice show increased serum adiponectin level compared to
491 wild type mice^{27; 42}. Importantly, increased serum adiponectin levels have been shown to be
492 protective in several pre-clinical models of angiogenesis in the eye, including models of
493 neovascular AMD⁴³⁻⁴⁵ and there is human genetic data linking adiponectin ADIPOQ and its
494 receptor ADIPOR1 to the risk of advanced AMD^{46; 47}. Finally, CIDEA, ADIPOQ and APOE
495 (an AMD GWAS locus also involved in lipid metabolism) have been linked as part of an 8-
496 gene hub identified as candidate serum biomarkers for diabetic peripheral neuropathy¹⁶.

497 In conclusion, our rare variant burden genetic analysis followed by our *in vitro*
498 dissection of the functional consequences of the beneficial variants, altogether with published
499 data, suggest that once patients have developed advanced AMD, the disease outcome could be
500 modified by systemic and indirect lipidomic biological processes that it would be interesting to
501 investigate further. In particular, investigating adipokines serum level, including adiponectin,

502 in advanced AMD patients could provide new biomarkers of neovascular AMD progression or
503 response to anti-VEGF therapy.

504

505

506 **Materials and Methods**

507 **Research subjects and low-luminance deficit (LLD)**

508 Before execution of the study, an internal Genentech team of Informed Consent Form
509 (ICF) experts reviewed the ICFs from all the studies to ensure appropriate use of the samples.
510 The HARBOR clinical trial (ClinicalTrials.gov identifier: NCT00891735) was a 24-month
511 Phase III study designed to evaluate the effectiveness of monthly or as-needed ranibizumab
512 delivery in patients with subfoveal neovascular AMD. This study has been described
513 previously^{13; 14}. LLD dysfunction is quantified by first assessing best corrected visual acuity
514 (BCVA) under normal lighting conditions, followed immediately by a low-luminance visual
515 acuity (LLVA) measurement, and this has been described previously^{11; 12}.

516 **Patient population and genetic analysis**

517 As we are looking at baseline characteristics, all HARBOR patients, regardless of
518 randomized treatment assignment, were eligible for inclusion in our study. We excluded
519 patients who did not consent for exploratory analyses and patients of non-European descent.
520 This resulted in the removal of 118 individuals from the overall enrolled trial study population,
521 representing 10.7% of the study population. We stratified patients for analysis based on LLD
522 quartile 1 (Q1) vs quartile 4 (Q4) as described previously¹². This resulted in 275 patients in our
523 Q1 group, and 241 patients in Q4. Further demographic information is found in **Table 1**.
524 Logistic regression was used to assess the association in the common variant analysis, adjusted

525 for age, sex, baseline visual acuity and genetically determined ancestry. PLINK version
526 1.90b3.46 was used for the common variant analysis.

527 The sequence data was annotated using SnpEff and there were 120,580 exonic coding variants
528 at a minor allele frequency < 1%. For a gene to be included in the analysis, it had to contain at
529 least two coding SNPs, resulting in 13,046 genes that could be tested for rare-variant gene-
530 burden. The rare variant gene burden test was used to assess the cumulative effect of rare
531 variants. Rvtest software (version 20170228) was used for the combined multivariate and
532 collapsing gene burden test, adjusted for age, sex, baseline visual acuity and genetically
533 determined ancestry. The rare variant gene burden test was used to assess the cumulative effect
534 of rare variants (MAF < 1%).

535 **Cell culture and treatments**

536 293T cells (ATCC #CRL-3216) and 3T3-L1 preadipocytes (ATCC #CL-173) were
537 cultured in Dulbecco's modified Eagle's Medium (DMEM) containing 10% fetal bovine serum
538 (FBS) and Penicillin (10,000 units/ml)/ Streptomycin (10,000µg/ml, 1:100 dilution of stock,
539 Gibco #15140-122). After reaching confluency, 3T3-L1 pre-adipocytes were cultured for 48
540 hours in DMEM + 10% FBS. The culture medium was then replaced by DMEM + 10% FBS +
541 5 µg/ml insulin (Sigma, I0516) + 1 µM dexamethasone (G-bioscience, API-04) + 0.5 mM
542 isobutylmethylxanthine (Sigma, I5879)] to induce adipocyte differentiation. After 48 hours, the
543 medium was replaced by DMEM + 10% FBS + 5 µg/ml insulin for an additional 48-72 hours
544 to achieve complete differentiation. To induce lipid droplet formation, cells were treated with
545 200 µM of oleic acid-albumin from bovine serum (Sigma, O3008). Human fetal retinal pigment
546 epithelial cells (hFRPE, Lonza #00194987) were cultured in RtEGM with supplement medium
547 as indicated by the manufacturer's protocol (RtEGM bullet kit, Lonza, #00195409). hFRPE
548 cells were cultured to high confluence on coverglass culture plates (Thermo, 155411) for three

549 weeks to obtain polarized RPE monolayers. After differentiation, hRPE cells were treated with
550 20 μ M A2E (*N*-Retinylidene-*N*-Retinylethanolamine, 20mM stock dissolved in DMSO, Gene
551 and Cell Technologies) for 24 hours.

552 **Plasmids, transfection and viruses.**

553 3x Flag- and GFP-tagged expression plasmids were used to express human CIDEC wild
554 type (WT) and the CIDEC rare variants (E186X, V47I, Y61H, V161M, or Q220H)
555 (Genecopoeia, Inc.). GFP- and mCherry-tagged plasmids were used to express human PLIN1,
556 AS160, and RAB8A (Genecopoeia, Inc.). 293T and 3T3-L1 cells were transiently transfected
557 using Lipofectamine2000 and Lipofectamine3000 (Invitrogen, 11668 and L3000). Expression
558 of GFP-tagged CIDEC in hRPE cells was carried out using lentivirus infection. Viral media
559 were collected from 293T cells transiently transfected with viral vector (expression plasmid),
560 delta8.9, and VSV-G in a molar ratio of 1:2.3:0.2 using Lipofectamine2000. HfRPE cells were
561 infected (without polybrene) on the day when they were split onto 6 well culture apparatuses
562 and kept in viral media for 4-5 days.

563 **Immunofluorescence, Immunoprecipitation and Immunoblotting**

564 Anti-Flag (Sigma, F7425), anti-GFP (Abcam, ab6556), anti-mCherry (Abcam,
565 ab167453) antibodies were obtained from commercial sources. Alexa 488-, Alexa-594-
566 conjugated secondary antibodies were obtained from Invitrogen. HRP-labeled secondary
567 antibodies were purchased from Cell Signaling Technologies. Cells were fixed with 4%
568 Paraformaldehyde (EMS, 15710S) for 15 minutes and mounted using ProLong Gold anti-fade
569 mounting medium with DAPI (Thermo Scientific, P36941). Images were obtained with a Nikon
570 A1R confocal microscope or Yokogawa CSU-X spinning disk on a Nikon TiE microscope and
571 a Photometrics Prime 95B. Image acquisition was performed using the NIS elements software
572 4.50 (Nikon). Co-immunoprecipitation was performed on 293T cells lysed in IP Lysis buffer

573 (Pierce #87788) containing a proteasome inhibitor cocktail (Pierce, Thermo Scientific, 87788)
574 two days after transient transfection. The cell lysates were incubated with anti-Flag M2 affinity
575 beads (Sigma, F2426) overnight at 4°C. After pull-down of the agarose beads, the
576 immunoprecipitates were washed three times with IP Lysis buffer and eluted in a 2x BOLT
577 Lithium dodecyl sulfate sample buffer for Western blot analysis. The samples were
578 electrophoresed on NuPage 4–12% Bis-Tris gels (Invitrogen #NP0303) in MES-SDS running
579 buffer (Invitrogen, #NP0002) and transferred to PVDF membrane (Invitrogen, #IB24001) for
580 immunoblotting.

581 **Lipid droplet (LD) assays**

582 3T3-L1 preadipocytes were fixed, stained with the LD marker Bodipy 558/568 C12
583 fatty acid (Molecular Probes, D3835) and LD diameters were measured in 100 to 150 cells from
584 three independent experiments using Imaris software (Bitplane) and Matlab image processing
585 toolkit. For live cell imaging, 3T3-L1 preadipocytes were transiently co-transfected with GFP-
586 tagged CIDEC and PLIN1-mCherry as LD markers, and incubated with 200 μ M of oleic acid.
587 Images were taken using the Nikon TiE spinning disk confocal microscope with an
588 environmental chamber (Okolab) for 12 hours in 5-minute intervals. The frequency of LD
589 fusion per cell and the time duration of LD fusion from three independent experiments were
590 quantified and plotted using Microsoft Excel 2011 and Graphpad Prism version 8.0.1.
591 Fluorescence Recovery After Photobleaching (FRAP)-based lipid diffusion assays were
592 conducted on the Nikon A1R confocal microscope. FRAP was performed on 3T3-L1
593 preadipocytes transiently transfected with GFP-tagged CIDEC were incubated with 200 μ M of
594 oleic acid and stained with Bodipy 558/568 C12 fatty acid (Molecular Probes, D3835) for 15
595 hours. One hour before the beginning of the FRAP assay, the medium was changed. LD pairs
596 with clear GFP expression at the contact sites were selected for bleaching. Selected regions

597 were bleached with a 561 nm laser at 100% power for 62.4 milliseconds, followed by time-
598 lapse scanning of 20-second intervals. Mean optical intensity (MOI) of the bleached and the
599 unbleached adjacent LD was measured by ImageJ and plotted using Microsoft Excel 2011 and
600 Graphpad Prism version 8.0.1.

601 **Mitochondria assays**

602 3T3-L1 cells expressing GFP-tagged human CIDEC were incubated with MitoTracker
603 (#M7512; Thermo Fisher Scientific) before fixation, followed by permeabilization with 0.5%
604 Triton X-100 and staining with DAPI. The mitochondrial density of the CIDEC-expressing
605 cells was determined by measuring the fluorescent intensity of the MitoTracker signal using
606 ImageJ. For the Seahorse Cell Mito Stress Test, 3T3-L1 cells expressing GFP or GFP-tagged
607 CIDEC WT and rare variants (V47I, Y61H, V161M, Q220H, and E186X) were plated on a 96-
608 well assay plate (10^4 cells/well). The cells were maintained in XF assay medium (Agilent,
609 #102365100) and subjected to a mitochondrial stress test, using the extracellular flux assay kit
610 by sequentially applying oligomycin (2 mmol/L), carbonyl cyanide 4-(trifluoromethoxy)
611 phenylhydrazone (FCCP; 5 mmol/L), and antimycin/rotenone (1 mmol/L and 1 mmol/L) (Cell
612 Mito Stress Test Kit, Agilent, #103015100). Analysis was carried out by using the Seahorse
613 analyzer software.

614 **In situ hybridization**

615 The *in situ* hybridization (ISH) BaseScope™ v2 assay (Advanced Cell Diagnostics
616 (ACD)) was performed on 5 µm-thick formalin-fixed paraffin-embedded sections of adult
617 human eyes according to the BaseScope™ detection reagent kit v2 ACD protocol. Probes
618 against the ubiquitously expressed isomerase PPIB were used as positive control, and probes
619 against bacterial DapB were used as negative control. Six custom probes of 18–25 bp
620 oligonucleotide sequences were designed by ACD for highly specific and sensitive detection of

621 human CIDEA RNA. After deparaffinization in xylene and endogenous peroxidase activity
622 inhibition by H₂O₂ (10 min), sections were permeabilized and submitted to heat (15 min at
623 100°C) and protease IV treatment (20 min at 40°C). After probe hybridization for 2 hours at
624 40°C, the signal was chemically amplified using the kit reagents and detected using the
625 FastRED dye. The sections were then counterstained with Hematoxylin and mounted using
626 VectaMount (Vector Labs, H-5000).

627 **Clinical images**

628 As part of the HARBOR clinical trial (NCT00891735)¹³, color fundus photographs,
629 fluorescein angiography, and spectral-domain optical coherence tomography images (Cirrus;
630 Carl Zeiss Meditec, Inc., Dublin, CA) were collected.

631 **Statistics for the *in vitro* analysis**

632 Data are reported as the means ± standard deviation for the indicated number of
633 experiments. At least three biological replicates were obtained for each experiment. Statistical
634 analysis was carried out using the Prism v9 software. Statistical significance of continuous data
635 was tested by the two-tailed Student's t-test. $p < 0.05$ was considered statistically significant.

636 **Web Resources**

637 dbSNP: <https://www.ncbi.nlm.nih.gov/snp>

638 Ensembl: http://grch37.ensembl.org/Homo_sapiens/Info/Index

639 OMIM: <http://www.omim.org/>

640 Uniprot: <https://www.uniprot.org/>

641 GTEx: <https://www.gtexportal.org/home/>

642 PolyPhen2: <http://genetics.bwh.harvard.edu/pph2/>

643 UK Biobank: <https://www.ukbiobank.ac.uk/>

644 Genebase: <https://genebase.org/>

645

646 **Data availability**

647 All reagents used in this study are commercially available and supplier names/catalog numbers
648 are provided in the Materials and Methods section of the manuscript. Human subjects were part
649 of the HARBOR clinical trial, ClinicalTrials.gov identifier: NCT00891735, and the study
650 population has been previously described for low-luminance deficit (LLD):

651 Frenkel, R.E., Shapiro, H., and Stoilov, I. (2016). Predicting vision gains with anti-VEGF
652 therapy in neovascular age-related macular degeneration patients by using low-luminance
653 vision. *The British journal of ophthalmology* 100, 1052-1057

654 <http://doi.org/10.1136/bjophthalmol-2015-307575>

655 Individual genetic data and other privacy-sensitive individual information are not publicly
656 available because they contain information that could compromise research participant privacy.

657 All publicly available code and software has been identified in the methods section of the
658 manuscript. We are unable to share genome-wide individual level data, even de-identified, due
659 to restrictions on the patient consents, however, all the summary statistics for the genetics
660 analysis can be provided upon request to the corresponding author (Dr Marion Jeanne:
661 jeanne.marion@gene.com) and/or the lead Human Geneticist (Dr Brian Yaspan:
662 yaspan.brian@gene.com). Data is available for qualified researcher employed or legitimately
663 affiliated with an academic, non-profit or government institution who have a track record in the
664 field. We would ask the researcher to sign a data access agreement that needs to be signed by
665 applicants and legal representatives of their institution, as well as legal representatives of
666 Genentech, Inc. A brief research proposal will be needed to ensure that 'Applications for access
667 to Data must be Specific, Measurable, Attainable, Resourced and Timely.'

668 The following previously published datasets were used:

669 1. Human Retina and RPE/Choroid bulk RNA sequencing, data from:
670 Orozco, L.D., Chen, H.H., Cox, C., Katschke, K.J., Jr., Arceo, R., Espiritu, C., Caplazi, P.,
671 Nghiem, S.S., Chen, Y.J., Modrusan, Z., et al. (2020). Integration of eQTL and a Single-Cell
672 Atlas in the Human Eye Identifies Causal Genes for Age-Related Macular Degeneration. Cell
673 Rep 30, 1246-1259 e1246.
674 <https://doi.org/10.1016/j.celrep.2019.12.082>

675 2. Human eye single cell RNA sequencing, data from:
676 Gautam, P., Hamashima, K., Chen, Y., Zeng, Y., Makovoz, B., Parikh, B.H., Lee, H.Y., Lau,
677 K.A., Su, X., Wong, R.C.B., et al. (2021). Multi-species single-cell transcriptomic analysis of
678 ocular compartment regulons. Nat Commun 12, 5675.
679 <https://doi.org/10.1038/s41467-021-25968-8>

680

681 **Acknowledgments**

682 We thank all of our Genentech colleagues involved in the Human Genetics Initiative including
683 Julie Hunkapiller, Jens Reeder, and Suresh Selvaraj. We also thank our colleagues in the
684 Research Pathology department, including Patrick Caplazi and Susan Haller.

685

686 **Competing interests**

687 At the time of the study, all authors were full time employees of Genentech/Roche with stock
688 and stock options in Roche. The funders had no role in study design, data collection and
689 interpretation, or the decision to submit the work for publication.

690

691 **Supplemental files:**

692 Uploaded as 5 additional files:

- 693 1. Supplemental Figures S1 to S5 and Supplemental Table S1 (PDF file)
- 694 2. Supplemental Table S2 (xls file)
- 695 3. Source data file: Figure 6 – Source data 1 (PDF file) Uncropped scans of the films used
- 696 to build figure 6 A, B, C and D. The area used in Figure 6 are highlighted on each film
- 697 by red rectangles.
- 698 4. Reporting standards from the EQUATOR network: GRIPS checklist (PDF file)
- 699 5. MDAR checklist (PDF file)

700

701 **Rich media file:**

702 Figure 4 – Video 1: Example of a representative time-lapse video of a lipid droplet fusion event in pre-

703 adipocytes expressing GFP-CIDEA wild-type (green) and mCherry-tagged PLIN1 (red).

704

705 **References**

- 706 1. Wong, W.L., Su, X., Li, X., Cheung, C.M., Klein, R., Cheng, C.Y., and Wong, T.Y. (2014).
- 707 Global prevalence of age-related macular degeneration and disease burden
- 708 projection for 2020 and 2040: a systematic review and meta-analysis. *Lancet*
- 709 *Glob Health* 2, e106-116.
- 710 2. Amoaku, W.M., Chakravarthy, U., Gale, R., Gavin, M., Ghanchi, F., Gibson, J., Harding, S.,
- 711 Johnston, R.L., Kelly, S.P., Lotery, A., et al. (2015). Defining response to anti-VEGF
- 712 therapies in neovascular AMD. *Eye (Lond)* 29, 721-731.
- 713 3. Klein, M.L., Mauldin, W.M., and Stoumbos, V.D. (1994). Heredity and age-related
- 714 macular degeneration. Observations in monozygotic twins. *Archives of*
- 715 *ophthalmology* 112, 932-937.
- 716 4. Meyers, S.M., Greene, T., and Gutman, F.A. (1995). A twin study of age-related macular
- 717 degeneration. *American journal of ophthalmology* 120, 757-766.
- 718 5. Hammond, C.J., Webster, A.R., Snieder, H., Bird, A.C., Gilbert, C.E., and Spector, T.D.
- 719 (2002). Genetic influence on early age-related maculopathy: a twin study.
- 720 *Ophthalmology* 109, 730-736.
- 721 6. Seddon, J.M., Ajani, U.A., and Mitchell, B.D. (1997). Familial aggregation of age-related
- 722 maculopathy. *American journal of ophthalmology* 123, 199-206.
- 723 7. Heiba, I.M., Elston, R.C., Klein, B.E., and Klein, R. (1994). Sibling correlations and
- 724 segregation analysis of age-related maculopathy: the Beaver Dam Eye Study.
- 725 *Genetic epidemiology* 11, 51-67.

- 726 8. Seddon, J.M., Cote, J., Page, W.F., Aggen, S.H., and Neale, M.C. (2005). The US twin study
727 of age-related macular degeneration: relative roles of genetic and environmental
728 influences. *Archives of ophthalmology* 123, 321-327.
- 729 9. Fritsche, L.G., Igl, W., Bailey, J.N., Grassmann, F., Sengupta, S., Bragg-Gresham, J.L.,
730 Burdon, K.P., Hebbring, S.J., Wen, C., Gorski, M., et al. (2016). A large genome-wide
731 association study of age-related macular degeneration highlights contributions of
732 rare and common variants. *Nat Genet* 48, 134-143.
- 733 10. Sunness, J.S., Rubin, G.S., Applegate, C.A., Bressler, N.M., Marsh, M.J., Hawkins, B.S.,
734 and Haselwood, D. (1997). Visual function abnormalities and prognosis in eyes
735 with age-related geographic atrophy of the macula and good visual acuity.
736 *Ophthalmology* 104, 1677-1691.
- 737 11. Sunness, J.S., Rubin, G.S., Broman, A., Applegate, C.A., Bressler, N.M., and Hawkins, B.S.
738 (2008). Low luminance visual dysfunction as a predictor of subsequent visual
739 acuity loss from geographic atrophy in age-related macular degeneration.
740 *Ophthalmology* 115, 1480-1488, 1488 e1481-1482.
- 741 12. Frenkel, R.E., Shapiro, H., and Stoilov, I. (2016). Predicting vision gains with anti-
742 VEGF therapy in neovascular age-related macular degeneration patients by using
743 low-luminance vision. *The British journal of ophthalmology* 100, 1052-1057.
- 744 13. Busbee, B.G., Ho, A.C., Brown, D.M., Heier, J.S., Suner, I.J., Li, Z., Rubio, R.G., Lai, P., and
745 Group, H.S. (2013). Twelve-month efficacy and safety of 0.5 mg or 2.0 mg
746 ranibizumab in patients with subfoveal neovascular age-related macular
747 degeneration. *Ophthalmology* 120, 1046-1056.
- 748 14. Ho, A.C., Busbee, B.G., Regillo, C.D., Wieland, M.R., Van Everen, S.A., Li, Z., Rubio, R.G.,
749 Lai, P., and Group, H.S. (2014). Twenty-four-month efficacy and safety of 0.5 mg
750 or 2.0 mg ranibizumab in patients with subfoveal neovascular age-related
751 macular degeneration. *Ophthalmology* 121, 2181-2192.
- 752 15. Auer, P.L., and Lettre, G. (2015). Rare variant association studies: considerations,
753 challenges and opportunities. *Genome Med* 7, 16.
- 754 16. Zhou, H., and Zhang, W. (2019). Gene expression profiling reveals candidate
755 biomarkers and probable molecular mechanism in diabetic peripheral
756 neuropathy. *Diabetes Metab Syndr Obes* 12, 1213-1223.
- 757 17. Karczewski, K.J., Solomonson, M., Chao, K.R., Goodrich, J.K., Tiao, G., Lu, W., Riley-
758 Gillis, B.M., Tsai, E.A., Kim, H.I., Zheng, X., et al. (2021). Systematic single-variant
759 and gene-based association testing of 3,700 phenotypes in 281,850 UK Biobank
760 exomes. *medRxiv*, 2021.2006.2019.21259117.
- 761 18. Carithers, L.J., Ardlie, K., Barcus, M., Branton, P.A., Britton, A., Buia, S.A., Compton,
762 C.C., DeLuca, D.S., Peter-Demchok, J., Gelfand, E.T., et al. (2015). A Novel Approach
763 to High-Quality Postmortem Tissue Procurement: The GTEx Project. *Biopreserv*
764 *Biobank* 13, 311-319.
- 765 19. Adzhubei, I.A., Schmidt, S., Peshkin, L., Ramensky, V.E., Gerasimova, A., Bork, P.,
766 Kondrashov, A.S., and Sunyaev, S.R. (2010). A method and server for predicting
767 damaging missense mutations. *Nat Methods* 7, 248-249.
- 768 20. Liang, L., Zhao, M., Xu, Z., Yokoyama, K.K., and Li, T. (2003). Molecular cloning and
769 characterization of CIDE-3, a novel member of the cell-death-inducing DNA-
770 fragmentation-factor (DFF45)-like effector family. *Biochem J* 370, 195-203.
- 771 21. Chapman, A.B., Knight, D.M., Dieckmann, B.S., and Ringold, G.M. (1984). Analysis of
772 gene expression during differentiation of adipogenic cells in culture and

- 773 hormonal control of the developmental program. *The Journal of biological*
774 *chemistry* 259, 15548-15555.
- 775 22. Danesch, U., Hoeck, W., and Ringold, G.M. (1992). Cloning and transcriptional
776 regulation of a novel adipocyte-specific gene, FSP27. CAAT-enhancer-binding
777 protein (C/EBP) and C/EBP-like proteins interact with sequences required for
778 differentiation-dependent expression. *The Journal of biological chemistry* 267,
779 7185-7193.
- 780 23. Puri, V., Konda, S., Ranjit, S., Aouadi, M., Chawla, A., Chouinard, M., Chakladar, A., and
781 Czech, M.P. (2007). Fat-specific protein 27, a novel lipid droplet protein that
782 enhances triglyceride storage. *The Journal of biological chemistry* 282, 34213-
783 34218.
- 784 24. Nishino, N., Tamori, Y., Tateya, S., Kawaguchi, T., Shibakusa, T., Mizunoya, W., Inoue,
785 K., Kitazawa, R., Kitazawa, S., Matsuki, Y., et al. (2008). FSP27 contributes to
786 efficient energy storage in murine white adipocytes by promoting the formation
787 of unilocular lipid droplets. *J Clin Invest* 118, 2808-2821.
- 788 25. Toh, S.Y., Gong, J., Du, G., Li, J.Z., Yang, S., Ye, J., Yao, H., Zhang, Y., Xue, B., Li, Q., et al.
789 (2008). Up-regulation of mitochondrial activity and acquirement of brown
790 adipose tissue-like property in the white adipose tissue of fsp27 deficient mice.
791 *PLoS One* 3, e2890.
- 792 26. Rubio-Cabezas, O., Puri, V., Murano, I., Saudek, V., Semple, R.K., Dash, S., Hyden, C.S.,
793 Bottomley, W., Vigouroux, C., Magre, J., et al. (2009). Partial lipodystrophy and
794 insulin resistant diabetes in a patient with a homozygous nonsense mutation in
795 CIDEA. *EMBO Mol Med* 1, 280-287.
- 796 27. Zhou, L., Park, S.Y., Xu, L., Xia, X., Ye, J., Su, L., Jeong, K.H., Hur, J.H., Oh, H., Tamori, Y., et
797 al. (2015). Insulin resistance and white adipose tissue inflammation are
798 uncoupled in energetically challenged Fsp27-deficient mice. *Nat Commun* 6,
799 5949.
- 800 28. Sun, Z., Gong, J., Wu, H., Xu, W., Wu, L., Xu, D., Gao, J., Wu, J.W., Yang, H., Yang, M., et al.
801 (2013). Perilipin1 promotes unilocular lipid droplet formation through the
802 activation of Fsp27 in adipocytes. *Nat Commun* 4, 1594.
- 803 29. Walther, T.C., and Farese, R.V., Jr. (2009). The life of lipid droplets. *Biochim Biophys*
804 *Acta* 1791, 459-466.
- 805 30. Bersuker, K., Peterson, C.W.H., To, M., Sahl, S.J., Savikhin, V., Grossman, E.A., Nomura,
806 D.K., and Olzmann, J.A. (2018). A Proximity Labeling Strategy Provides Insights
807 into the Composition and Dynamics of Lipid Droplet Proteomes. *Dev Cell* 44, 97-
808 112 e117.
- 809 31. Gao, G., Chen, F.J., Zhou, L., Su, L., Xu, D., Xu, L., and Li, P. (2017). Control of lipid
810 droplet fusion and growth by CIDE family proteins. *Biochim Biophys Acta Mol*
811 *Cell Biol Lipids* 1862, 1197-1204.
- 812 32. Wu, C., Zhang, Y., Sun, Z., and Li, P. (2008). Molecular evolution of Cide family
813 proteins: novel domain formation in early vertebrates and the subsequent
814 divergence. *BMC Evol Biol* 8, 159.
- 815 33. Wu, L., Xu, D., Zhou, L., Xie, B., Yu, L., Yang, H., Huang, L., Ye, J., Deng, H., Yuan, Y.A., et
816 al. (2014). Rab8a-AS160-MSS4 regulatory circuit controls lipid droplet fusion and
817 growth. *Dev Cell* 30, 378-393.
- 818 34. Orozco, L.D., Chen, H.H., Cox, C., Katschke, K.J., Jr., Arceo, R., Espiritu, C., Caplazi, P.,
819 Nghiem, S.S., Chen, Y.J., Modrusan, Z., et al. (2020). Integration of eQTL and a

- 820 Single-Cell Atlas in the Human Eye Identifies Causal Genes for Age-Related
821 Macular Degeneration. *Cell Rep* 30, 1246-1259 e1246.
- 822 35. Gautam, P., Hamashima, K., Chen, Y., Zeng, Y., Makovoz, B., Parikh, B.H., Lee, H.Y., Lau,
823 K.A., Su, X., Wong, R.C.B., et al. (2021). Multi-species single-cell transcriptomic
824 analysis of ocular compartment regulons. *Nat Commun* 12, 5675.
- 825 36. Imanishi, Y., Batten, M.L., Piston, D.W., Baehr, W., and Palczewski, K. (2004).
826 Noninvasive two-photon imaging reveals retinyl ester storage structures in the
827 eye. *J Cell Biol* 164, 373-383.
- 828 37. McBee, J.K., Palczewski, K., Baehr, W., and Pepperberg, D.R. (2001). Confronting
829 complexity: the interlink of phototransduction and retinoid metabolism in the
830 vertebrate retina. *Prog Retin Eye Res* 20, 469-529.
- 831 38. Song, F.Q., Zhou, H.M., Ma, W.X., Li, Y.L., Hu, B.A., Shang, Y.Y., Wang, Z.H., Zhong, M.,
832 Zhang, W., and Ti, Y. (2022). CIDEc: A Potential Factor in Diabetic Vascular
833 Inflammation. *J Vasc Res* 59, 114-123.
- 834 39. Rajamoorthi, A., Lee, R.G., and Baldan, A. (2018). Therapeutic silencing of FSP27
835 reduces the progression of atherosclerosis in *Ldlr*(-/-) mice. *Atherosclerosis* 275,
836 43-49.
- 837 40. van Leeuwen, E.M., Emri, E., Merle, B.M.J., Colijn, J.M., Kersten, E., Cougnard-Gregoire,
838 A., Dammeier, S., Meester-Smoor, M., Pool, F.M., de Jong, E.K., et al. (2018). A new
839 perspective on lipid research in age-related macular degeneration. *Prog Retin*
840 *Eye Res* 67, 56-86.
- 841 41. Tanaka, N., Takahashi, S., Matsubara, T., Jiang, C., Sakamoto, W., Chanturiya, T., Teng,
842 R., Gavrilova, O., and Gonzalez, F.J. (2015). Adipocyte-specific disruption of fat-
843 specific protein 27 causes hepatosteatosis and insulin resistance in high-fat diet-
844 fed mice. *The Journal of biological chemistry* 290, 3092-3105.
- 845 42. Zhou, L., Yu, M., Arshad, M., Wang, W., Lu, Y., Gong, J., Gu, Y., Li, P., and Xu, L. (2018).
846 Coordination Among Lipid Droplets, Peroxisomes, and Mitochondria Regulates
847 Energy Expenditure Through the CIDE-ATGL-PPARalpha Pathway in Adipocytes.
848 *Diabetes* 67, 1935-1948.
- 849 43. Lyzogubov, V.V., Tytarenko, R.G., Bora, N.S., and Bora, P.S. (2012). Inhibitory role of
850 adiponectin peptide I on rat choroidal neovascularization. *Biochim Biophys Acta*
851 1823, 1264-1272.
- 852 44. Fu, Z., Liegl, R., Wang, Z., Gong, Y., Liu, C.H., Sun, Y., Cakir, B., Burnim, S.B., Meng, S.S.,
853 Lofqvist, C., et al. (2017). Adiponectin Mediates Dietary Omega-3 Long-Chain
854 Polyunsaturated Fatty Acid Protection Against Choroidal Neovascularization in
855 Mice. *Investigative ophthalmology & visual science* 58, 3862-3870.
- 856 45. Li, H.Y., Hong, X., Cao, Q.Q., and So, K.F. (2019). Adiponectin, exercise and eye
857 diseases. *Int Rev Neurobiol* 147, 281-294.
- 858 46. Cao, G., Chen, Y., Zhang, J., Liu, Y., Zhang, M., Zhang, K., and Su, Z. (2015). Effects of
859 adiponectin polymorphisms on the risk of advanced age-related macular
860 degeneration. *Biomarkers* 20, 266-270.
- 861 47. Kaarniranta, K., Paananen, J., Nevalainen, T., Sorri, I., Seitsonen, S., Immonen, I.,
862 Salminen, A., Pulkkinen, L., and Uusitupa, M. (2012). Adiponectin receptor 1 gene
863 (*ADIPOR1*) variant is associated with advanced age-related macular degeneration
864 in Finnish population. *Neurosci Lett* 513, 233-237.
- 865

866

867 **Abbreviations:**

868 AMD: Age-related macular degeneration
869 AR: autosomal recessive
870 BCVA: best corrected visual acuity
871 CIDEA: Cell-death-Inducing DNA fragmentation factor (DFF)45-like Effector C
872 CNV: choroidal neovascularization
873 EST: Expressed Sequence Tag
874 FPLD5: Familial Partial Lipodystrophy type 5
875 GA: Geographic Atrophy
876 GWAS: Genome-wide association studies
877 IAMDC: International AMD Genetics Consortium
878 LD: lipid droplet
879 LLD: low-luminance deficit
880 LLVA: low-luminance visual acuity
881 MAF: minor allele frequency
882 MOI: mean optical intensity
883 OCT: Optical Coherence Tomography
884 OR: odds ratio
885 Q: quartile
886 RGCs: Retinal Ganglion Cells
887 RPE: Retinal Pigment Epithelium
888 SNP: single-nucleotide polymorphism
889 VEGF: Vascular Endothelial Growth Factor
890 WGS: whole genome sequencing
891 WT: wild-type
892

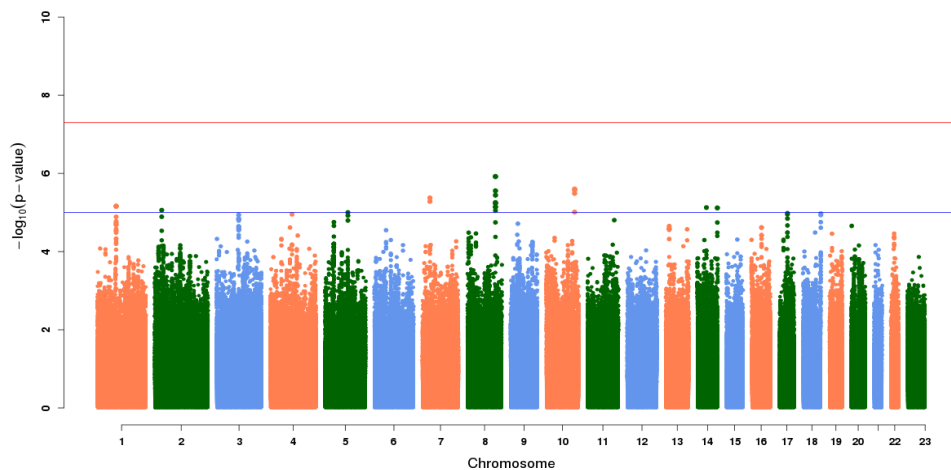


Figure S1: Manhattan plot of common variant analysis results contrasting AMD patients in the top and bottom LDD quartiles (Q1 and Q4).

In adipose tissue, only 0.5% of *CIDEC* transcripts contain exon 4

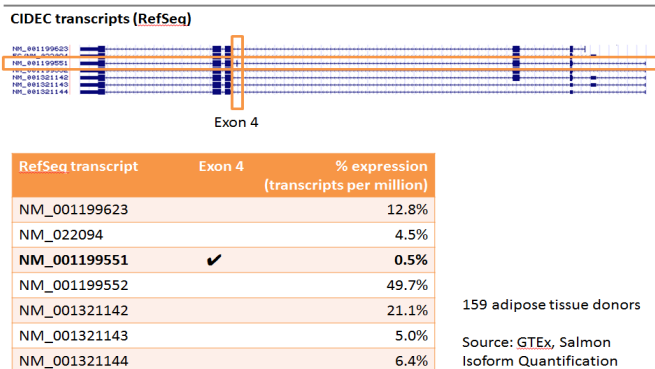


Figure S2: Summary of *CIDEC* exon expression in adipose tissue. *CIDEC* exon 4, the location of all rare variants seen in Q4 AMD patients, is expressed in 0.5% of all *CIDEC* transcripts found in adipose tissue in samples from the GTEx project.

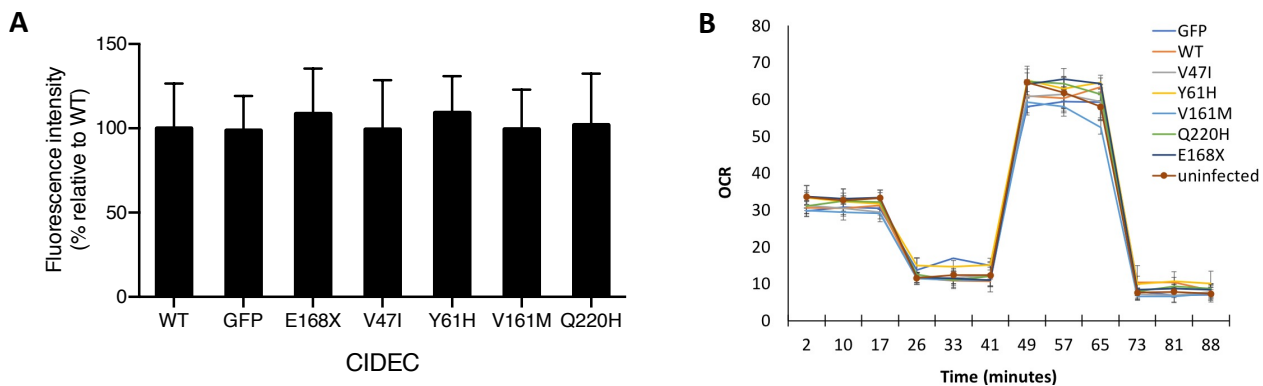


Figure S3: *CIDEC* rare variants do not affect mitochondria density or function. Quantification of mitochondria density using MitoTracker in 3T3-L1 cells expressing *CIDEC* wild-type (WT) or each of the rare variants (A). Mitochondria function measured by Seahorse analyzer (OCR: Oxygen consumption rate) (B).

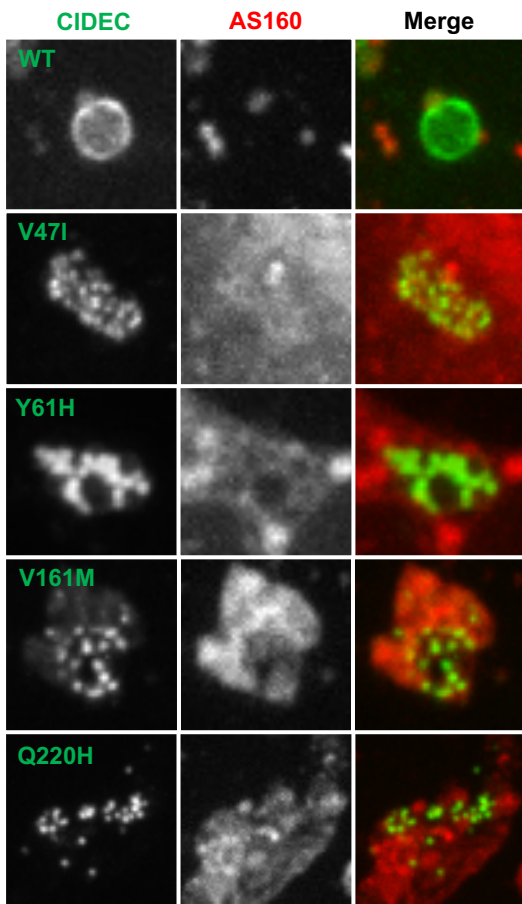


Figure S4: Representative images of CIDEC wild-type (WT) or rare variants (green) and AS160 (red) in pre-adipocytes.

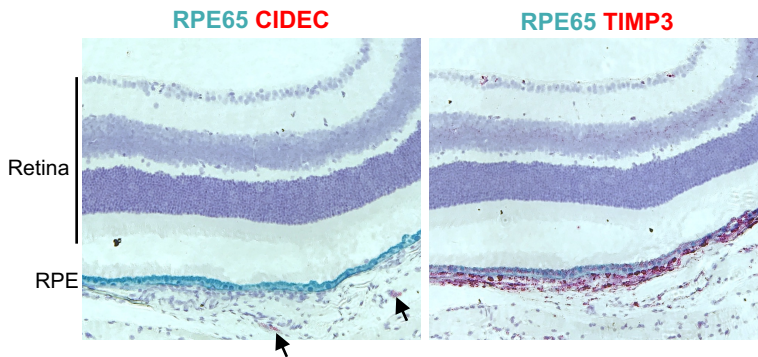


Figure S5: By in situ hybridization (ISH), Cidec RNA is not detected in mouse retina and Retinal Pigment Epithelium (RPE) cells. Rare Cidec positive cells are present in the choroidal tissue underneath the RPE (left: red, arrows). ISH for Rpe65 was used as RPE cell marker, and ISH for Timp3 (right: red) was used as positive control.

| SNP | LOCUS | CHR | BP | A1 | Q1 MAF | Q4 MAF | OR | p value |
|-------------|---------------------|-----|-----------|----|--------|--------|------|---------|
| rs10033900 | <i>CFI</i> | 4 | 109737911 | T | 0.47 | 0.52 | 0.83 | 0.20 |
| rs10781182 | <i>MIR6130-RORB</i> | 9 | 74002804 | T | 0.36 | 0.36 | 0.94 | 0.69 |
| rs10922109 | <i>CFH</i> | 1 | 196735502 | A | 0.26 | 0.23 | 1.10 | 0.47 |
| rs11080055 | <i>TMEM97-VTN</i> | 17 | 28322698 | A | 0.45 | 0.47 | 0.91 | 0.49 |
| rs114092250 | <i>PRLR-SPEF2</i> | 5 | 35494346 | A | 0.02 | 0.03 | 0.78 | 0.58 |
| rs1142 | <i>KMT2E-SRPK2</i> | 7 | 105115879 | T | 0.38 | 0.33 | 1.24 | 0.13 |
| rs12357257 | <i>ARHGAP21</i> | 10 | 24710664 | A | 0.20 | 0.29 | 0.63 | 0.004 |
| rs140647181 | <i>COL8A1</i> | 3 | 99461824 | C | 0.03 | 0.03 | 1.01 | 0.97 |
| rs1626340 | <i>TGFB1</i> | 9 | 99161090 | A | 0.17 | 0.20 | 0.90 | 0.54 |
| rs2043085 | <i>LIPC</i> | 15 | 58388755 | T | 0.40 | 0.35 | 1.29 | 0.10 |
| rs2230199 | <i>C3</i> | 19 | 6718376 | C | 0.28 | 0.27 | 0.99 | 0.96 |
| rs3138141 | <i>RDH5-CD63</i> | 12 | 55721994 | A | 0.20 | 0.25 | 0.79 | 0.17 |
| rs3750846 | <i>ARMS2-HTRA1</i> | 10 | 122456049 | C | 0.41 | 0.41 | 1.05 | 0.71 |
| rs429358 | <i>APOE</i> | 19 | 44908684 | C | 0.09 | 0.11 | 0.89 | 0.62 |
| rs5754227 | <i>SYN3-TIMP3</i> | 22 | 32709831 | C | 0.10 | 0.10 | 1.03 | 0.89 |
| rs61941274 | <i>ACAD10</i> | 12 | 111694806 | A | 0.03 | 0.04 | 0.75 | 0.48 |
| rs61985136 | <i>RAD51B</i> | 14 | 68302482 | C | 0.34 | 0.36 | 0.94 | 0.68 |
| rs62247658 | <i>ADAMTS9-AS2</i> | 3 | 64729479 | C | 0.45 | 0.50 | 0.83 | 0.18 |
| rs67538026 | <i>CNN2</i> | 19 | 1031439 | T | 0.46 | 0.48 | 0.93 | 0.62 |
| rs72802342 | <i>CTRB2-CTRB1</i> | 16 | 75200974 | A | 0.07 | 0.06 | 1.34 | 0.32 |
| rs7803454 | <i>PILRB-PILRA</i> | 7 | 100393925 | T | 0.21 | 0.20 | 1.25 | 0.20 |
| rs8135665 | <i>SLC16A8</i> | 22 | 38080269 | T | 0.21 | 0.20 | 1.04 | 0.83 |
| rs943080 | <i>VEGFA</i> | 6 | 43858890 | C | 0.45 | 0.43 | 1.10 | 0.50 |
| rs9564692 | <i>B3GALT1</i> | 13 | 31247103 | T | 0.28 | 0.25 | 1.21 | 0.22 |

Table S1: Comparison of AMD associated risk variants from Fritsche et. al, Nat Gen, 2015 in Q1 and Q4 AMD patients.

Table S2: (attached as a xls file): Results from UK Biobank rare variant burden PheWAS